Master's Thesis

석사 학위논문

Fabrication and characterization of magnetically actuated flexible microrobot based on guidewire for intravascular treatment

Jeonghun Lee (이 정 훈 李 政 勳)

Department of

Robotics Engineering

DGIST

2017

Master's Thesis

석사 학위논문

Fabrication and characterization of magnetically actuated flexible microrobot based on guidewire for intravascular treatment

Jeonghun Lee (이 정 훈 李 政 勳)

Department of

Robotics Engineering

DGIST

2017

Fabrication and characterization of magnetically actuated flexible micro-robot based on guidewire for intravascular treatment

Advisor : Professor Hongsoo Choi

Co-advisor : Professor Ji-Woong Choi

By

Jeonghun Lee

Department of Robotics Engineering

DGIST

A thesis submitted to the faculty of DGIST in partial fulfillment of the requirements for the degree of Master of Science in the Department of Robotics Engineering. The study was conducted in accordance with Code of Research Ethics[1]

01. 06. 2017

Approved by

Professor Hongsoo Choi (Signature)
(Advisor)

Professor Ji-Woong Choi (Signature)
(Co-Advisor)

[1] Declaration of Ethical Conduct in Research**:** I, as a graduate student of DGIST, hereby declare that I have not committed any acts that may damage the credibility of my research. These include, but are not limited to: falsification, thesis written by someone else, distortion of research findings or plagiarism. I affirm that my thesis contains honest conclusions based on my own careful research under the guidance of my thesis advisor.

Fabrication and characterization of magnetically actuated flexible microrobot based on guidewire for intravascular treatment

Jeonghun Lee

Accepted in partial fulfillment of the requirements for the degree of Master of Science.

01. 06. 2017

Head of Committee Prof. Hongsoo Choi (인)

Committee Member Prof. Ji-Woong Choi (인)

Committee Member Prof. Jonghyun Kim (인)

MS/RT

201523006

이 정 훈. Jeonghun Lee. Fabrication and characterization of magnetically actuated flexible microrobot based on guidewire for intravascular treatment. Department of Robotics Engineering. 2017. 87p. Advisors Prof. Choi, Hongsoo, Co-Advisors Prof. Choi, Ji-Woong.

ABSTRACT

In this research, medical microrobot based on guidewire was fabricated for intravascular treatment such as chronic total occlusion (CTO). Chronic total occlusion (CTO) is totally clogged vessel disease for two or more months. Percutaneous coronary intervention (PCI) procedure is conventional treatment method using medical tools such as guidewire, balloon catheter, and stent. Guidewire takes a role to be guidance toward the lesion in human body with path of blood vessel. However, this guidewire has low controllability due to manipulation by operator's hand. To increase controllability of guidewire for enhanced percutaneous coronary intervention (PCI) procedure, a flexible microrobot for medical tool was used at the guidewire. Structure of this flexible microrobot consist of the permanent magnet, beam, and connector. The proposed cylindrical microrobots were successfully fabricated by a replica molding method with polydimethylsiloxane (PDMS) material for formability, flexibility, and biocompatibility. This fabricated microrobot was attached to tip of guidewire using epoxy. Steering experiments of flexible microrobot were conducted by controlling external magnetic field. This magnetic field was generated by half-sphere type eight electromagnetic coil system (Minimag) using current control. Flexible microrobot was deformed toward all of direction under magnetic field. Deformation angle of flexible microrobot is maximum almost 80 degrees at the magnetic field with 15 mT of intensity and 170 degrees of direction. Also, this results were

compared with analytic solution driven by Euler-Bernoulli beam theory and finite element method (FEM) analysis of multiphysics modeling. Designed microrobot for improvement of performance of guidewire was conducted *in vitro* experiments in blood vessel phantom to confirm track-ability. Flexible microrobots was confirmed to success until 60 degrees of branch angle in blood vessel phantom. Also, Flexible microrobot based on guidewire was demonstrated in blood vessel networks phantom with multiple branch. This research confirmed the remotely steerable microrobot with magnetic actuation and track-ability of microrobot based on guidewire. Flexible microrobot based on guidewire was shown possibility of robotic assisted percutaneous coronary intervention (PCI) for intravascular treatment.

Keywords: Flexible microrobot, Replica molding method, Magnetic actuation, Finite element method (FEM), Intravascular treatment.

CONTENTS

List of Figures

List of tables

I. INTRODUCTION

1.1 Chronic total occlusion (CTO)

The blood vessel is important path to deliver the oxygen and nutrient for energy source toward cells in full body. This paths in human body were threatened the health due to stress, cholesterol, smoking, and obesity. The blood vessel was narrowed and blocked though these various factors [1]. Arteriosclerosis is the narrowed vessel diseases to be stacked cholesterol on endothelium which is placed on innermost structure of blood vessel (Figure 1.1). This narrowed blood vessel disturbs the passing blood flow. Abnormal blood flow can cause malfunction of organs and tissues in a body such as myocardium. Myocardial infarction is to be necrosis of muscular tissue and cells. Occurrence of myocardial infarction in the heart leads to death (Figure 1.2). Formation of this clogged blood vessel largely divided by two methods. Acute arterial occlusion (AAO) usually occur to be blocked in narrowed blood vessel with acute thrombus caused by rupture of atherosclerosis [2]. The other way is to be slowly progressed blockage caused by repetition between damage and recovery of vascular. Blockade in the latter case is called chronic total occlusion (CTO). CTO mean cardiovascular disease that CA was perfectly blockaded for two mouth or more (Figure 1.3) [3]. The CTO lesion is more rigid compared with AAO due to calcification for a long time.

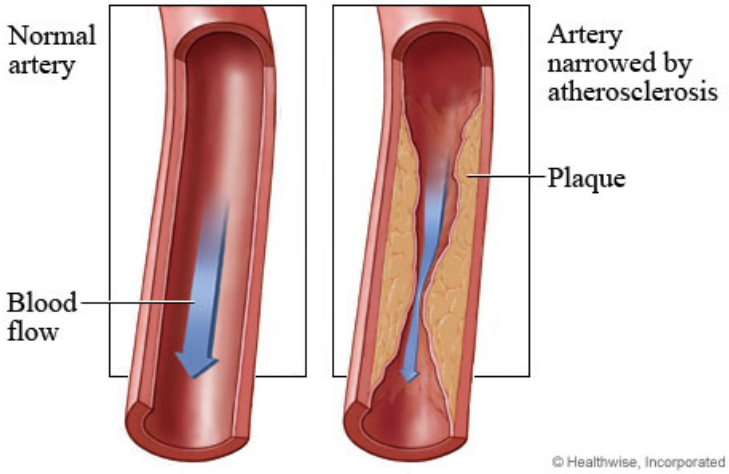

Figure 1.1 Arteriosclerosis

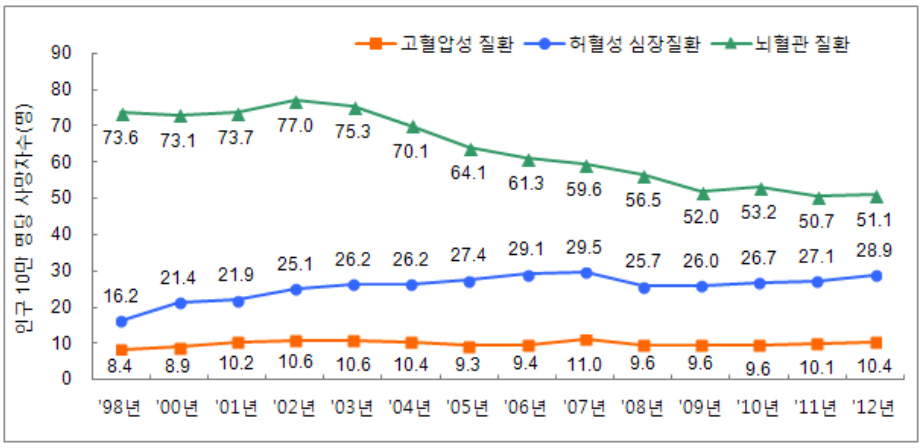

Figure 1.2 Annual death rate of circulation disease according to Ministry of Health-Welfare in South Korea; (Red) Hypertensive arteriopathy, (Blue) Ischemic heart diseases, (Green) Cerebrovascular disease

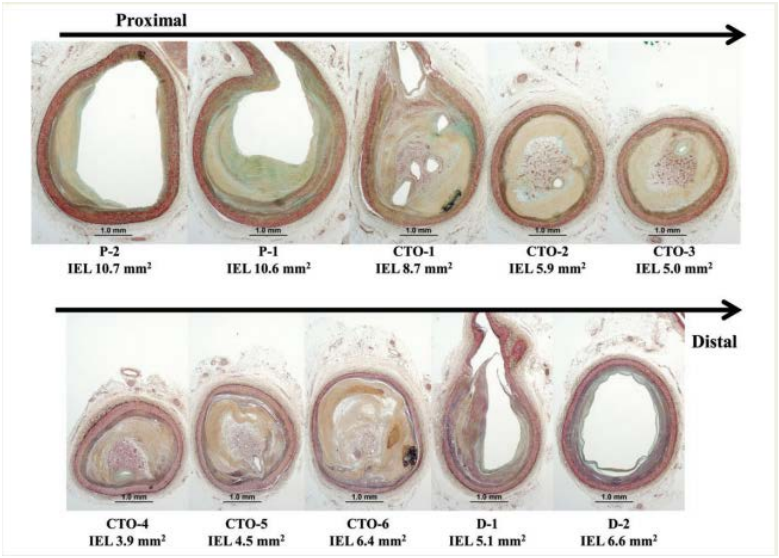

Figure 1.3 Cross-section of coronary artery with Chronic total occlusion [4]

1.2 Conventional surgery for treatment of blood vessel diseases

To treat these clogged vascular disease, there is usually divided by coronary artery bypass grafting surgery (CABG) and percutaneous coronary intervention (PCI) (Figure 1.4) [4]. Coronary artery bypass grafting surgery (CABG) is surgical procedure that detour for running the stopped blood stream in clogged blood vessel was built with the rarely used blood vessel, which is taken at own human body, instead of the blockaded vascular. Percutaneous coronary intervention (PCI) is a non-surgical procedure that various catheter and guidewire (GW) was moved to the lesion along with blood vessel path for treatment of vessel disease (Figure 1.5). Also, a various of drilling catheter for chronic total occlusion (CTO) were commercialized (Figure 1.6). Percutaneous coronary intervention (PCI) use X-ray imaging for confirmation of position of lesion and medical tools.

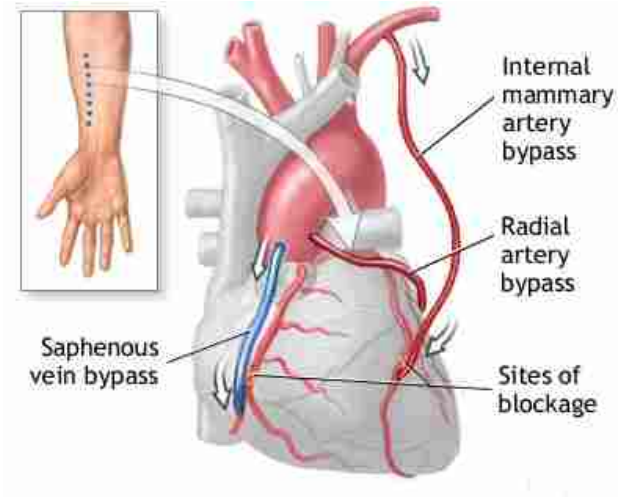

Figure 1.4 Coronary arteries bypass grafting (CABG) surgery

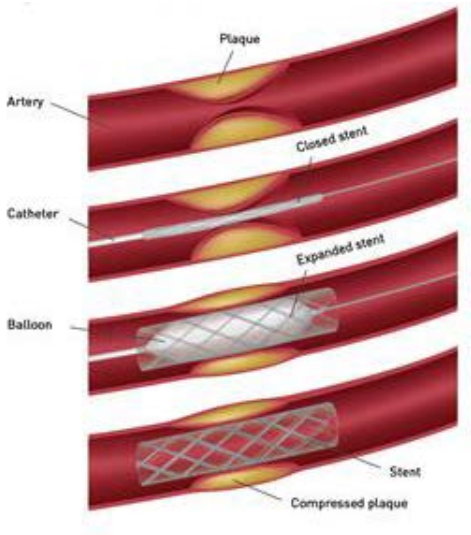

Figure 1.5 Percutaneous coronary intervention (PCI) procedure with guidewire, balloon catheter and stent for treatment of intravascular disease

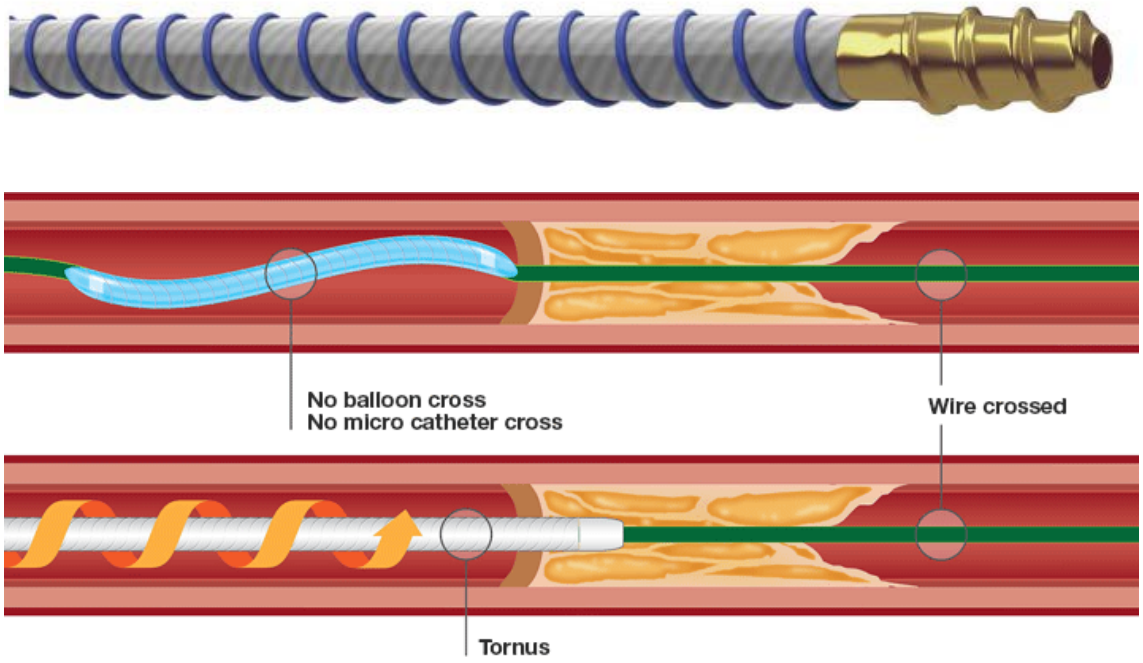

Figure 1.6 Catheter (Turnpike Gold catheter, Vascular Solutions Inc., USA) for treatment of chronic total occlusion (CTO) and schematic of drilling catheter

Coronary artery bypass grafting surgery (CABG) has been used for a long time and very difficult to operate for even a skilled clinician. Also, the open surgery was given negative effect to patient. To solve these problems, minimally invasive surgery (MIS) method was getting the limelight [5]. With advances in technology, Mohr et al proofed that percutaneous coronary intervention (PCI) is relatively more reasonable than coronary artery bypass grafting surgery (CABG) [6].

Guidewire (GW) is necessary tool for percutaneous coronary intervention (PCI) treatment (Figure 1.7). the well-developed conventional type consists of core wire for penetrating force and coils to transmit torque for rotation. tip of guidewire (GW) is simply controlled by manually pushing it back and forth or turning the guidewire (GW) about its axis [7]. This method takes a long time to move toward the desired position in a sharp bend or complicated vascular. Thus, a long operation leads to increase the radiation exposure for both doctor and patient due to angiography for a long time [8].

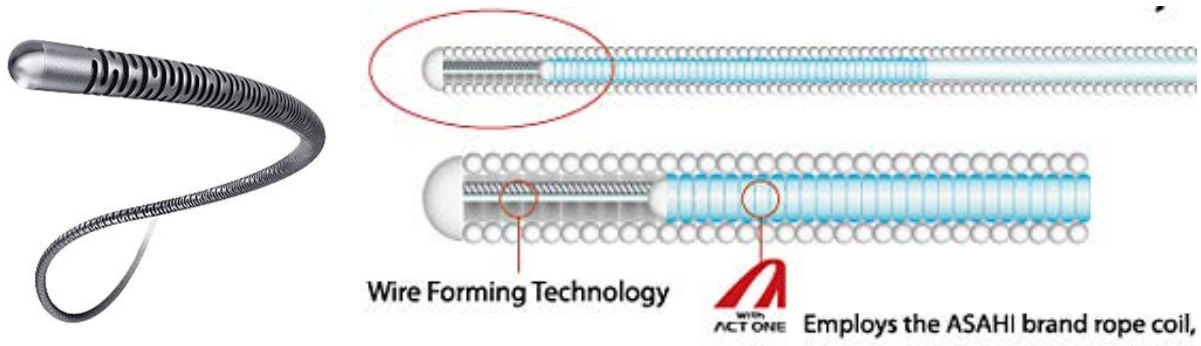

Figure 1.7 Guidewire and structure of guidewire (ASAHI SION, Asahi Intecc, Japan)

1.3 Micro-/nano-robots for biomedical application

In currently, a variety of robots have been developing for minimally invasive surgery (MIS) due to a positive effect of minimally invasive surgery (MIS) for patient such as reduction of recovery time and infection risks [5]. These robots have been decreased in mill scale to be able to swallow for treatment as well as in micro-/nano-scale to be move along to blood-vessel for transportation to lesion. Tiny robots were difficult to embed a power source for movement. To solve the issue, micro-/nano-robots is moved by a variable of force and torque such as magnetic, chemical reaction, and ultrasound [9-11]. In current, biomedical micro-/nano-robots have been developed to move toward desired direction as well as to add additional function [12]. Biomedical micro-/nano-robots is able to perform a variable of medical task for minimally invasive surgery (MIS) which include drug/cell delivery, hyperthermia, scaffolding, and ablation (Figure 1.8) [5].

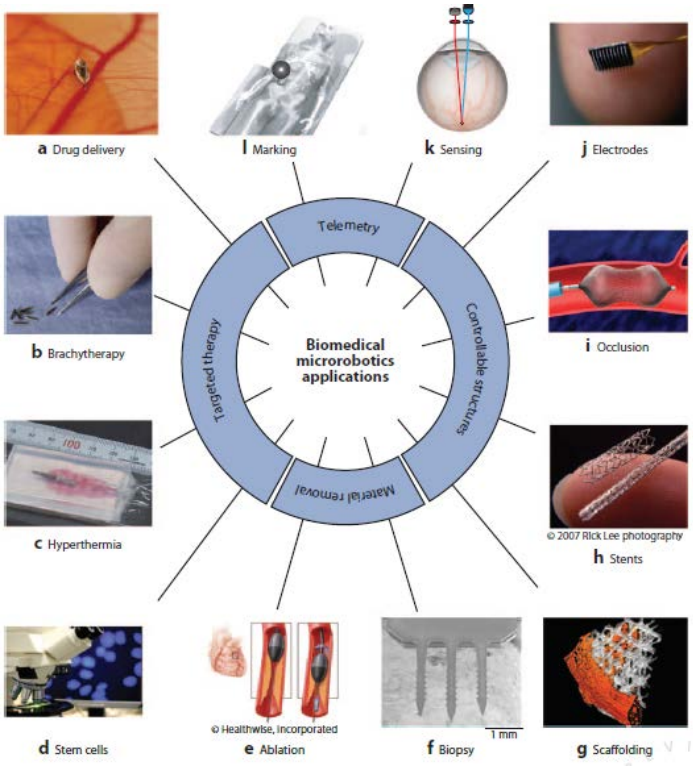

Figure 1.8 Medical tasks for microrobots [5]

Micro-/nano-robots for drug/cell delivery and ablation are appropriate to treat above mentioned intravascular diseases. Fibrinolytic drug delivery using micro-/nano-robots has advantage of reduction of abused drug. Research in tissue engineering field has been developing to recovery the damaged myocardium tissue with stem cells (Figure 1.9) [13, 14].

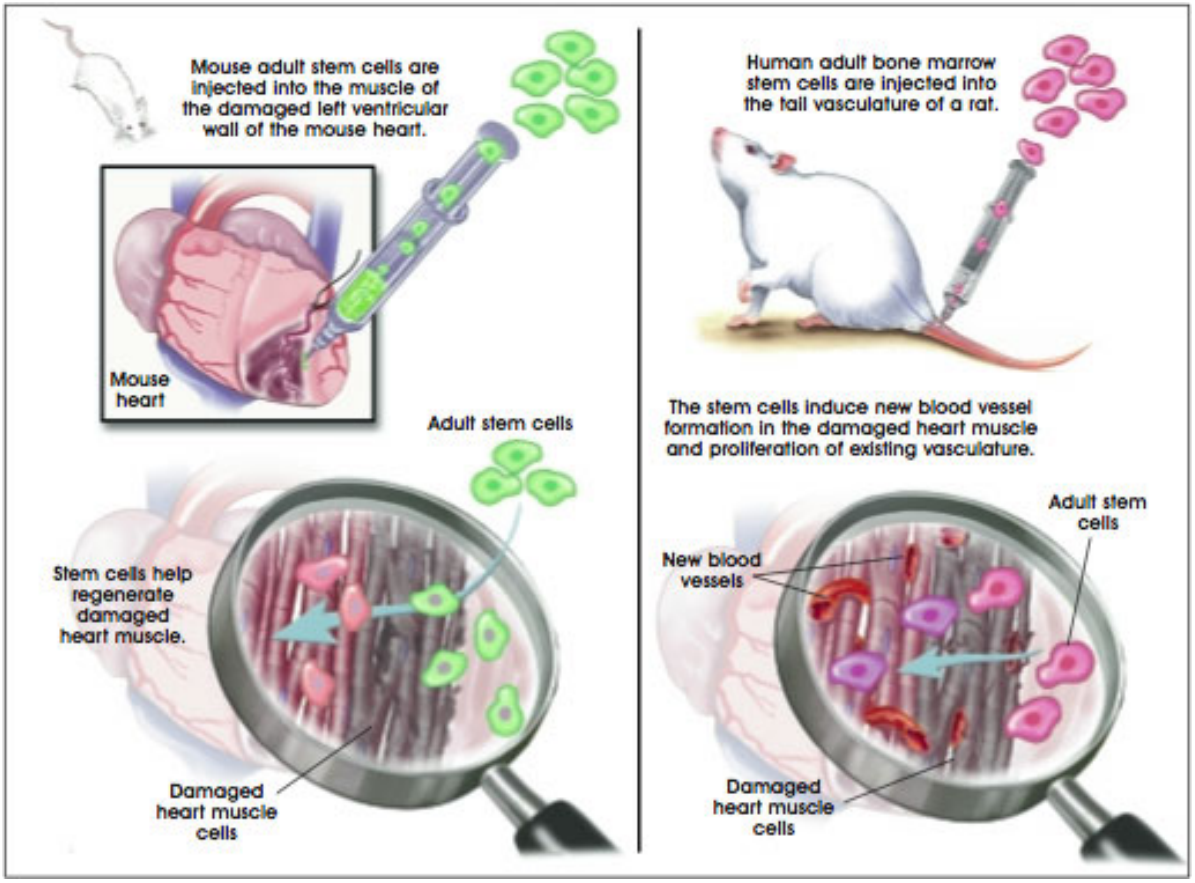

Figure 1.9 Recovery of myocardium using stem cells (© 2001 Terese Winslow, Lydia Kibiuk)

Transportation of stem cells using micro-/nano-robots is one of suitable methods for minimally invasive surgery (MIS) (Figure 1.10) [15]. Moving mechanism of micro-/nano-robots is that robots with helical shape are propelled due to corkscrew motion caused by rotating external magnetic field (Figure 1.11) [16-18]. The drilling microrobots with helical shape for intravascular treatment have been studying for penetrating artificial clogged blood vessel (Figure 1.12) [19].

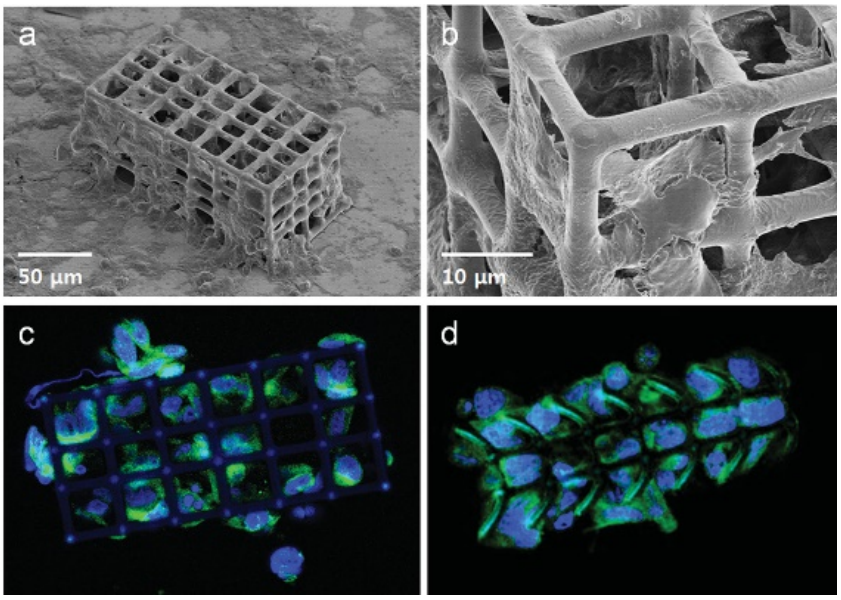

Figure 1.10 A hexahedral microrobot after stem cell culture [15]

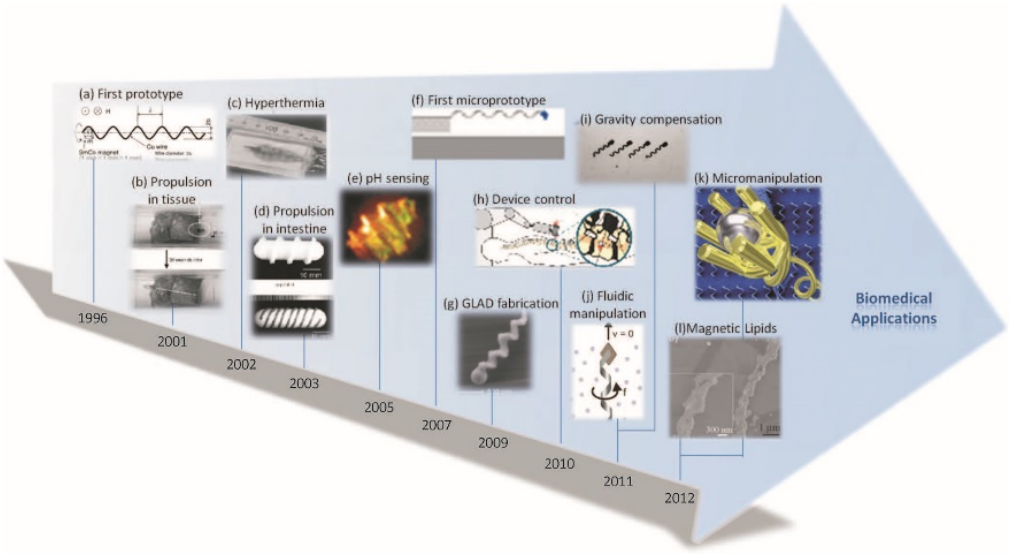

Figure 1.11 A history on magnetically actuated helical microrobots [16]

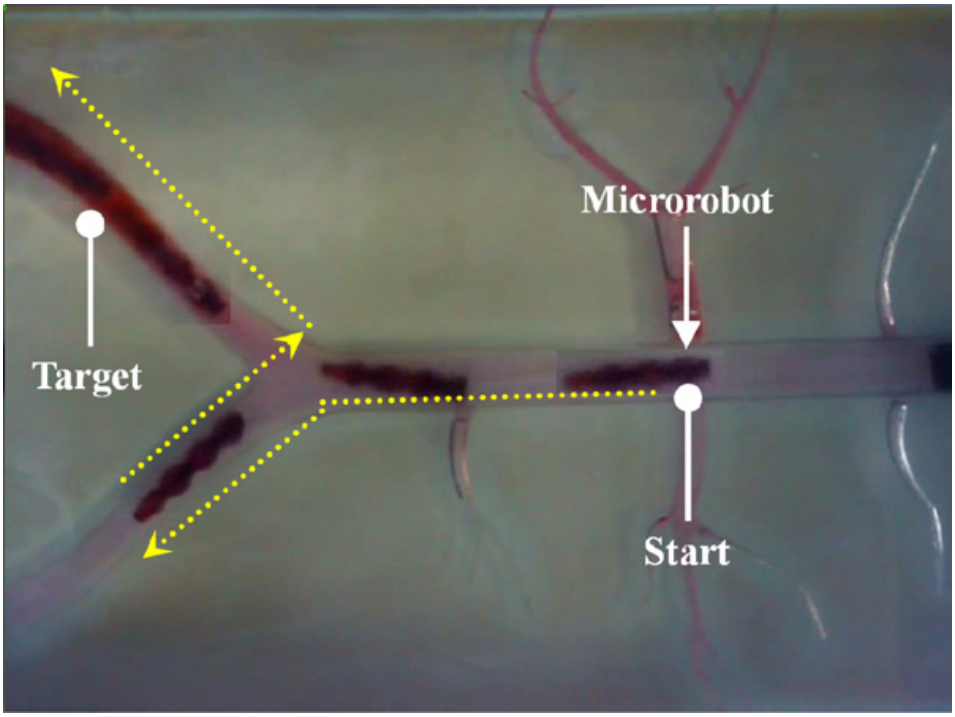

Figure 1.12 Experimental result of microrobot in blood vessel phantom [19]

In general, micro-/nano-robots has several issue to be recognize treatment method for human. In spite of swimming structure along the blood vessel in human body, almost biomedical microrobots were conducted medical task in static fluidic environment and have a lower one's velocity compared with blood flow. Secondary issue is retrieval of micro-robots. Micro-robots swim in working space within some centimeter due to limitation of magnetic field generating system. At the full-body system in human, biomedical microrobots is difficult to be returned toward inserted position. One solution is to connect between tip of wire and micro-robots for retrieval.

1.4 Soft Material for flexible microrobots

Polydimethylsiloxane (PDMS) have been fabricated for medical device due to a various of useful advantage in medical application. Polydimethylsiloxane (PDMS) is soft material with low young's modulus and high Poisson's ratio (Figure 1.13) [20-22].

In micro-electro mechanical systems (MEMS) technology, flexible devices such as tactile sensor attached at the skin were fabricated to need bended surface geometry with polydimethylsiloxane (PDMS) through performance of mechanical property (Figure 1.14) [23]. Polydimethylsiloxane (PDMS) was used at the fabrication of microrobots for non-symmetry actuation using elastic restoring force due to property of elastomer with high Poisson's ratio.

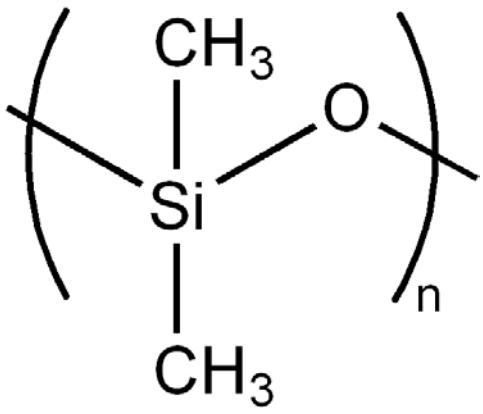

Figure 1.13 Chemical formula of polydimethylsiloxane (PDMS) Material

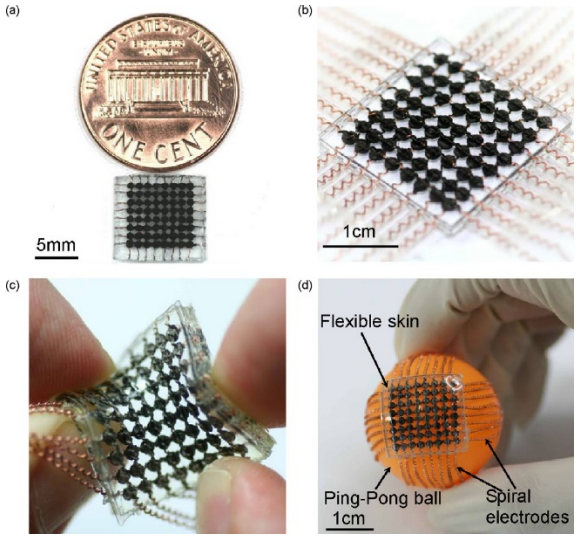

Figure 1.14 Flexible sensor [23]

This soft material has advantage of high formability. This property of polydimethylsiloxane (PDMS) material is useful at the fabrication of structure using replica molding method or stamping method. Micro-fluidic devices were fabricated with a desired structure, which is made by three dimensional (3D) printer or mechanical machining, and polydimethylsiloxane (PDMS) material in micro-electro mechanical system (MEMS) technology [24, 25]. A various of pillar structures were made by using the same fabrication process. Magnetically actuated devices with mixing between magnetic particle (MP) and polydimethylsiloxane (PDMS) were fabricated (Figure 1.15) [26-29]. Micro-electro mechanical system (MEMS) devices composed with magnetically actuated elastomer were used in actuator and sensors such as micro-motor, micro-valve, micro-sorter of micro fluidic channel [27, 30-33].

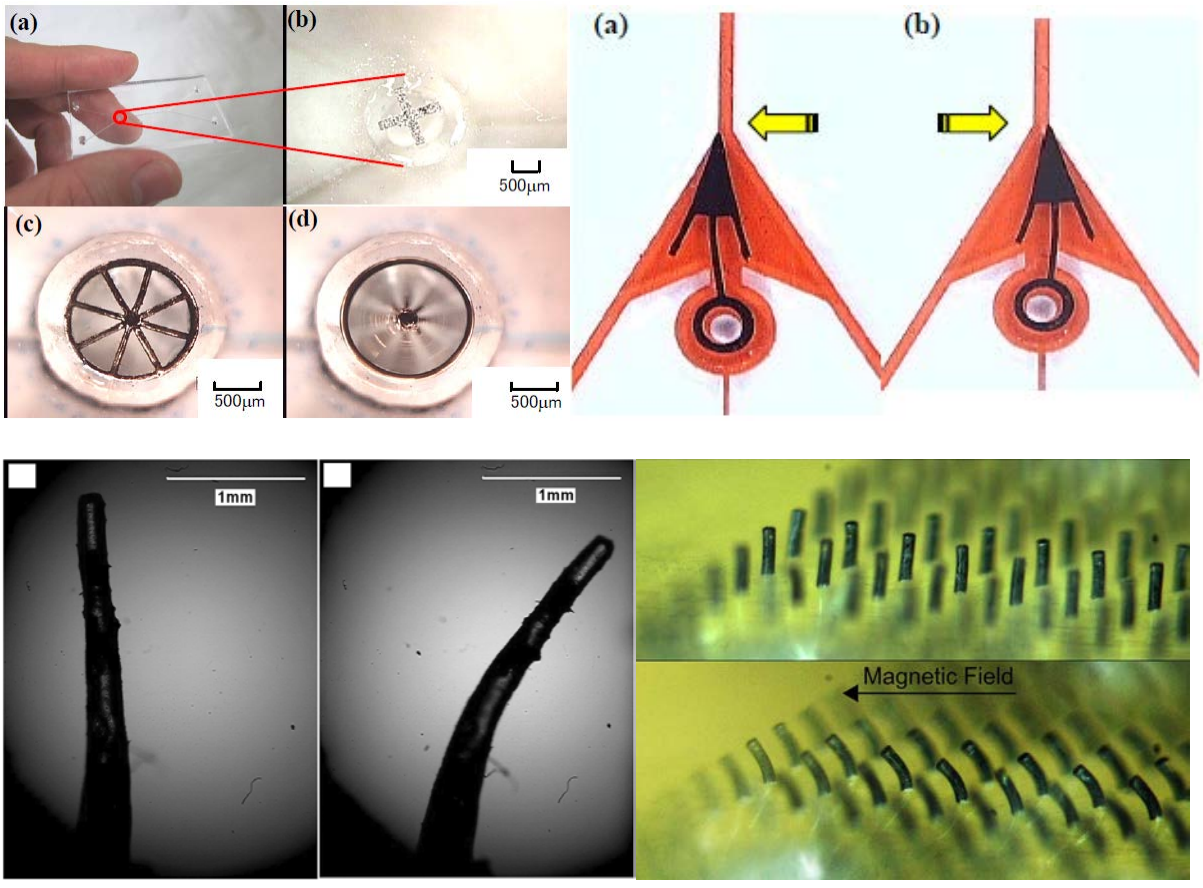

Figure 1.15 Magnetically actuated pillar structure [26-28]

Researches in biomedical field is important to use biocompatible material to eliminate cytotoxicity. Polydimethylsiloxane (PDMS) is typical biocompatible material. Container with biocompatible material is basically used for cell culture. Artificial blood vessel was fabricated with polydimethylsiloxane (PDMS) material due to biocompatibility (Figure 1.16) [24, 34]. Biomedical device for measuring contact force of cell was made using patterned polydimethylsiloxane (PDMS) sensor for mechanical characterization of cells and tissue with magnetic agent such as nanowires or nanoparticles (Figure 1.17) [35, 36]. Polydimethylsiloxane (PDMS) devices is suitable in biomedical application and has property of flexibility to bend.

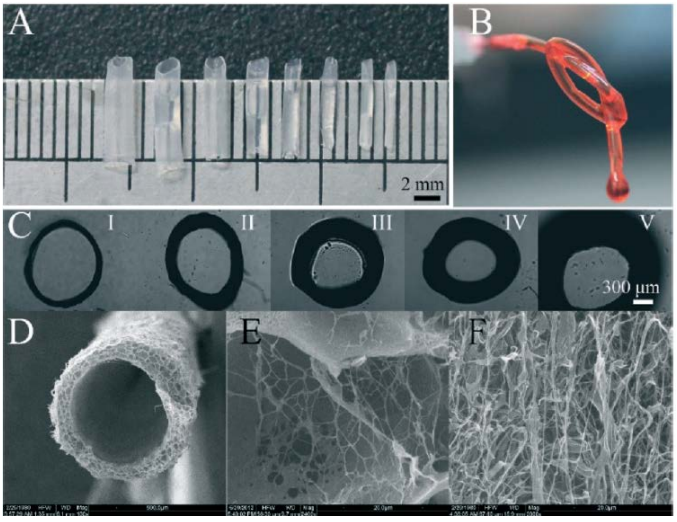

Figure 1.16 Artificial blood vessel composed with polydimethylsiloxane (PDMS) [24]

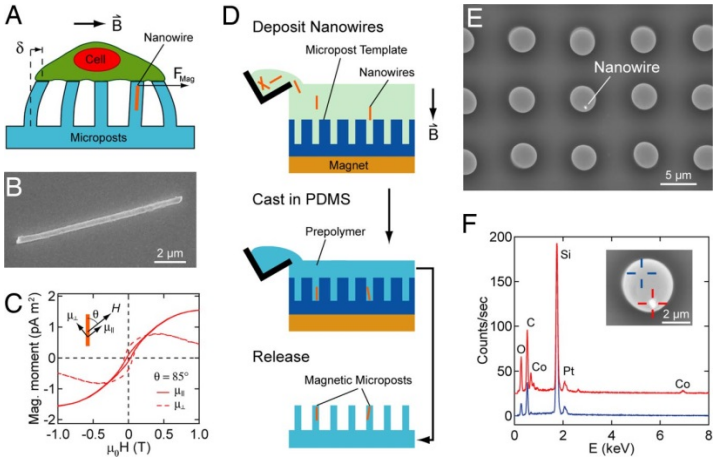

Figure 1.17 Microfabricated arrays of magnetic post [35]

1.5 Related research for remotely actuated guidewire (GW) and catheter

1.5.1 Exterior control system for intravascular treatment

Many researchers have attempted to conduct a delicate surgery and to solve a serious radiation exposure through cooperation with the robot. A solution for the problem is that surgeon transfer from operating room to the safety area from radiation exposure. These researches for solving problem approach two ways. One method is that a robot is used as a substitute for surgeon's hand. Systems for robotic catheterization consist of master and slave parts (Figure 1.18) [37, 38]. Master parts is sensor to measure manipulation of surgeon. Slave parts is actuator to control guidewire (GW) and catheter according to measured manipulation. These types robot (Sensei X Robotic catheter system, Hansen Medical) have been commercialized (Figure 1.19). In current research, operator felt as a directly handling surgery using haptic function through interwork between master and slave systems. However, robotic catheterization is easily influenced by a performance of medical tools such as stiffness of guidewire (GW) [39]. These approach way using exterior control system has limitation of controllability of actuated guidewire.

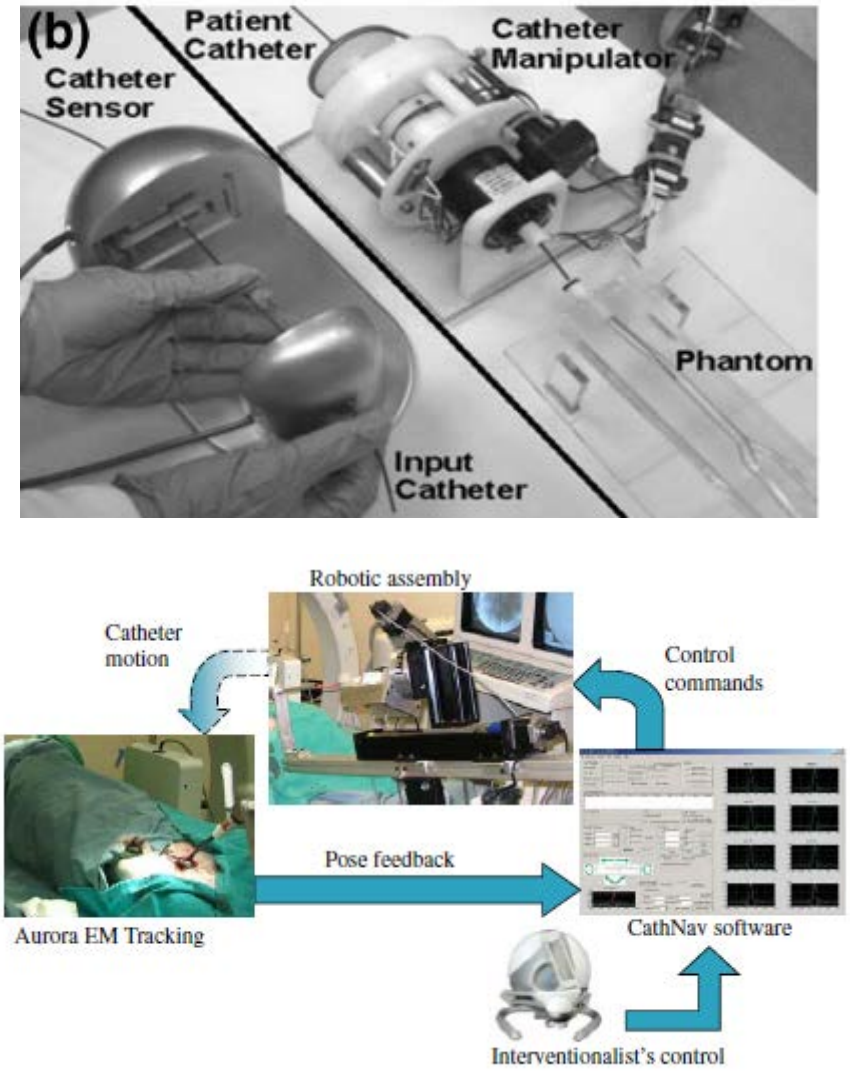

Figure 1.18 The robotic systems [37, 38]

Figure 1.19 Commercial master/slave system for robotic catheterization

1.5.2 Interior control system for intravascular treatment

Other approaching method is to use remotely steerable guidewire (GW) and catheter for increasing controllability. Actuated catheters are pull-wire type using mechanical force, magnetic steerable type using external magnetic field, smart material actuated type using shape memory alloy (SMA), and hydraulically-driven type using hydric pressure (Figure 1.20) [7]. Pull-wire type and hydraulically-driven type of these actuated catheters is difficult to apply at actuated guidewire (GW) with small diameter due to complexity of structure. Also, smart material actuated type has thermal problem and electric shock.

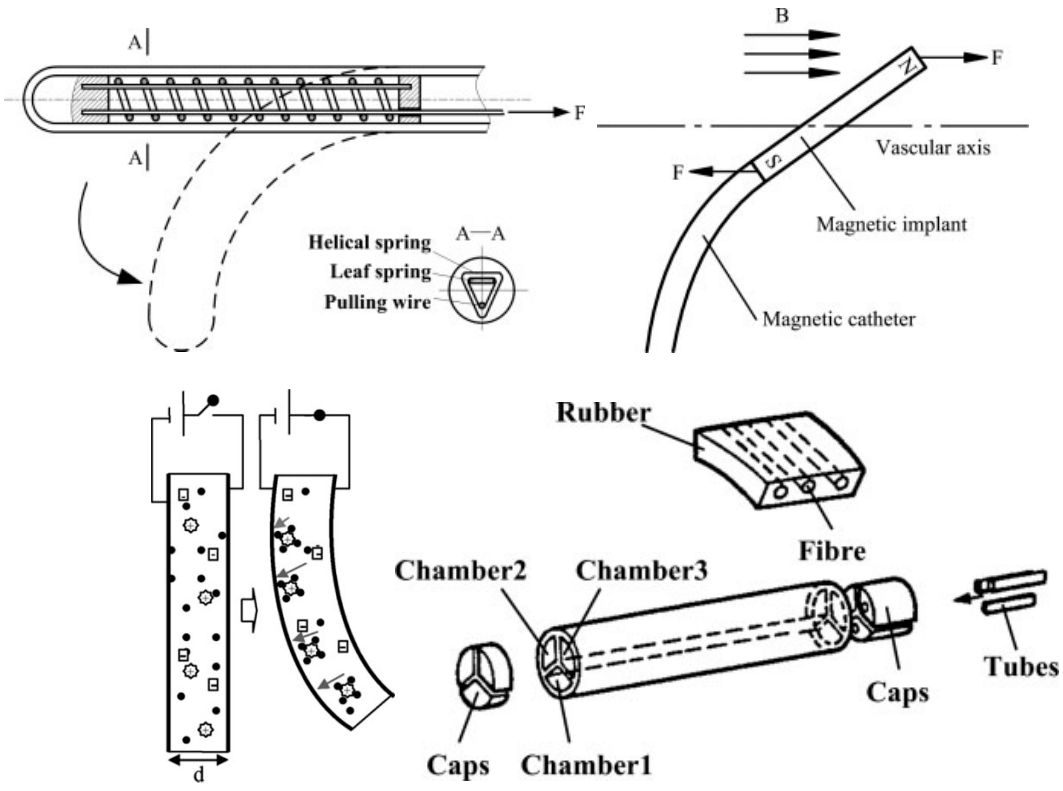

Figure 1.20 Actuated guidewires [7]

Magnetic field is harmless to humans and has been used medical device such as magnetic resonance imaging (MRI) equipment. Many researches have been developed about magnetic steerable catheter (Figure 1.21)[40-45]. The applied principle is to use alignment between magnetization direction of magnetic object and direction of external magnetic field [46]. Magnetically actuated guidewire (GW) and catheter were classified according to control method[7]. These methods are the permanent magnet attached at wire tip magnet under adjusting external magnetic field and controlling current of solenoid coil under constant magnetic field. To apply guidewire (GW), the permanent magnet type is more proper than solenoid type because of requirement of cable for suppling power.

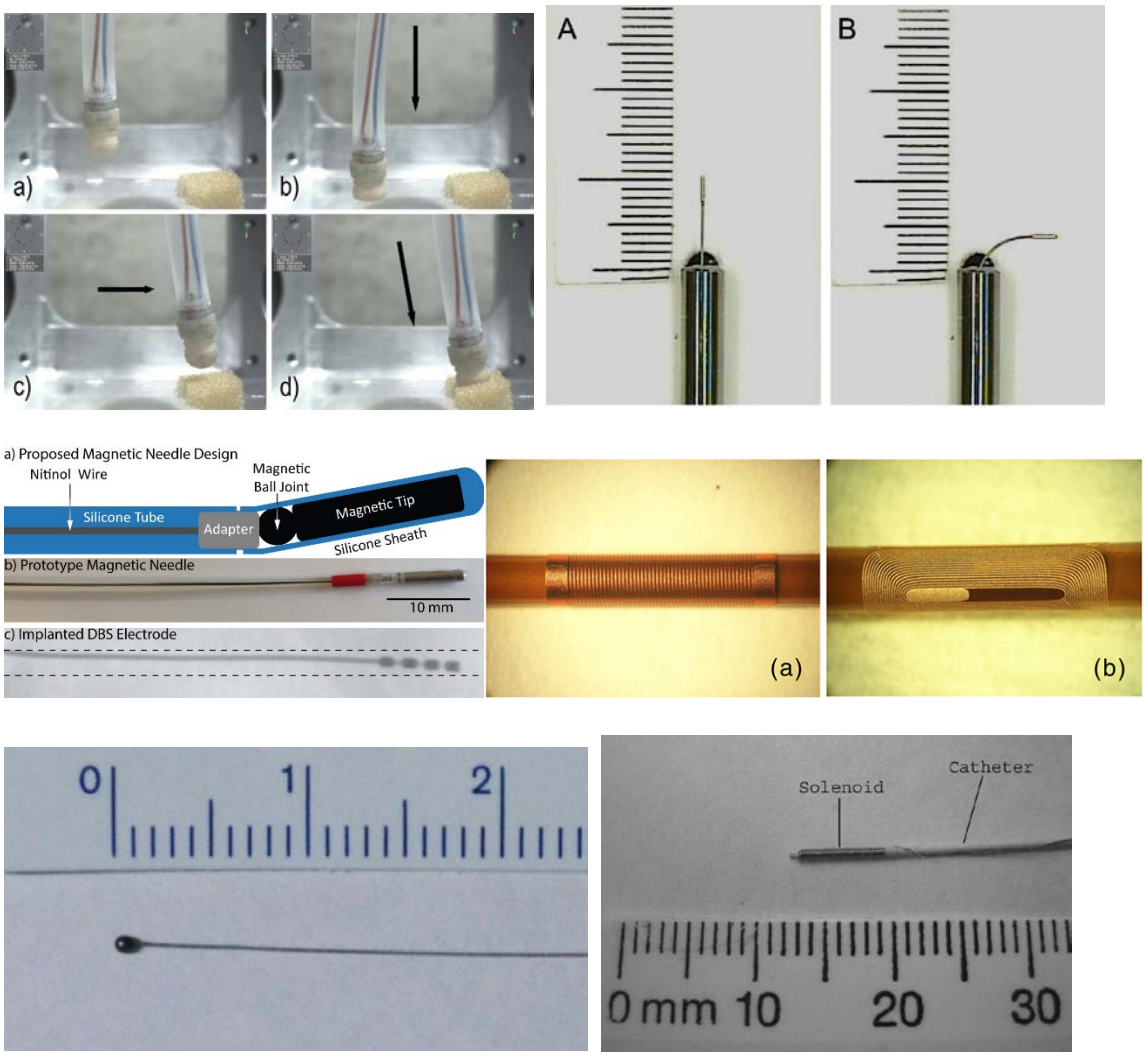

Figure 1.21 Magnetic catheters and guidewires (GW) [40-45]

Steerable catheter using permanent magnet was commercialized for treatment of arrhythmia which is cardiac diseases to be abnormally beating [47]. Many research was conduct animal test as well as clinic trial for treatment [47, 48]. Commercial magnetic steerable catheter (MSC) has one or more of permanent magnet at the tip and touch at the inner surface of heart for treatment[47, 49]. Magnetic field generator (MFG) is important to manipulate magnetic steerable catheter (MSC) for treatment of arrhythmia. Methods of magnetic field generator (MFG) are controlling position of the huge permanent magnet or current of multi-electromagnet coils [50-54]. In forward method, commercial magnetic field generates between two huge permanent magnets and is controlled by adjusting position and orientation of magnets (Figure 1.22) [41]. In different method, commercial 8-electromagnet coils, which are arranged in sphere area, generate magnetic field by controlling current (Figure 1.23) [55].

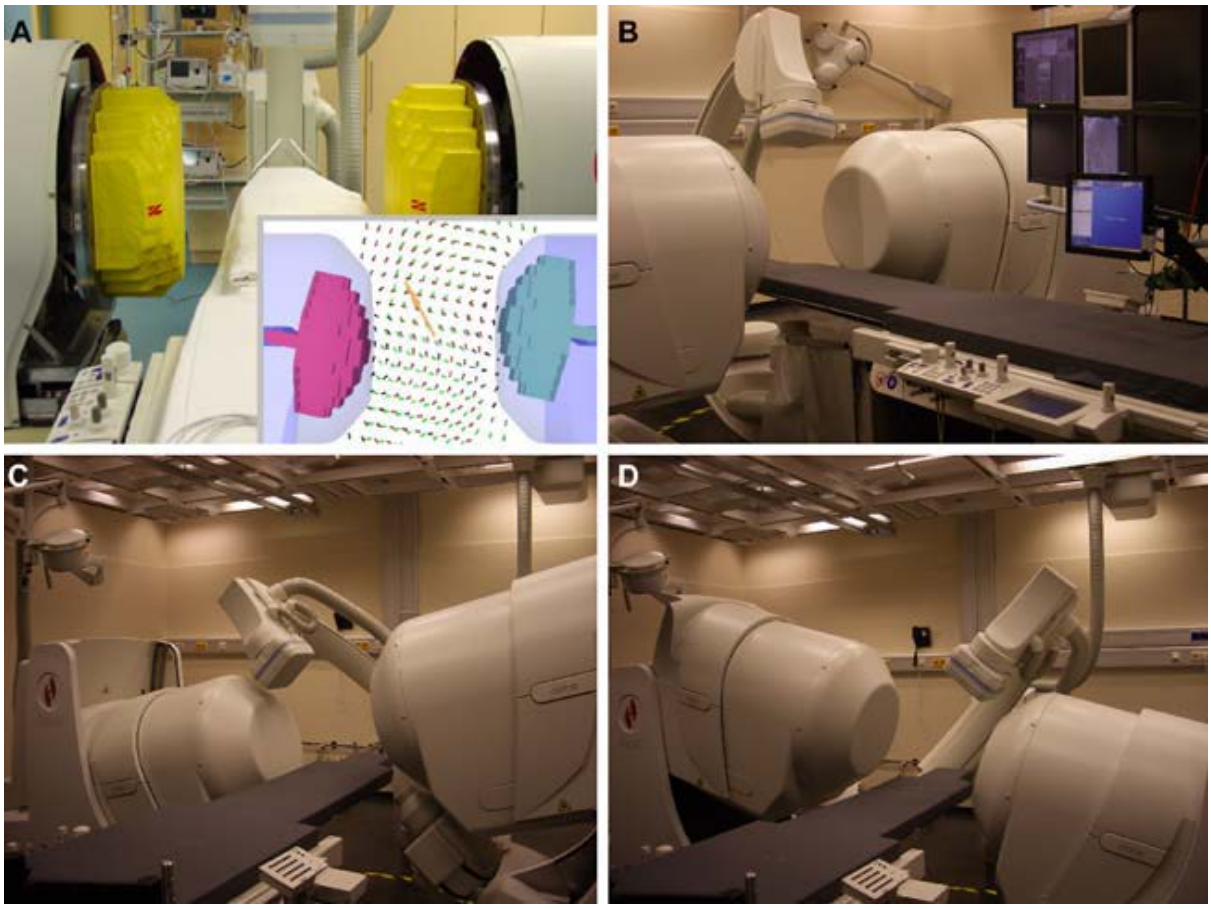

Figure 1.22 Magnetic field generator (MFG) controlling position of permanent magnet [41]

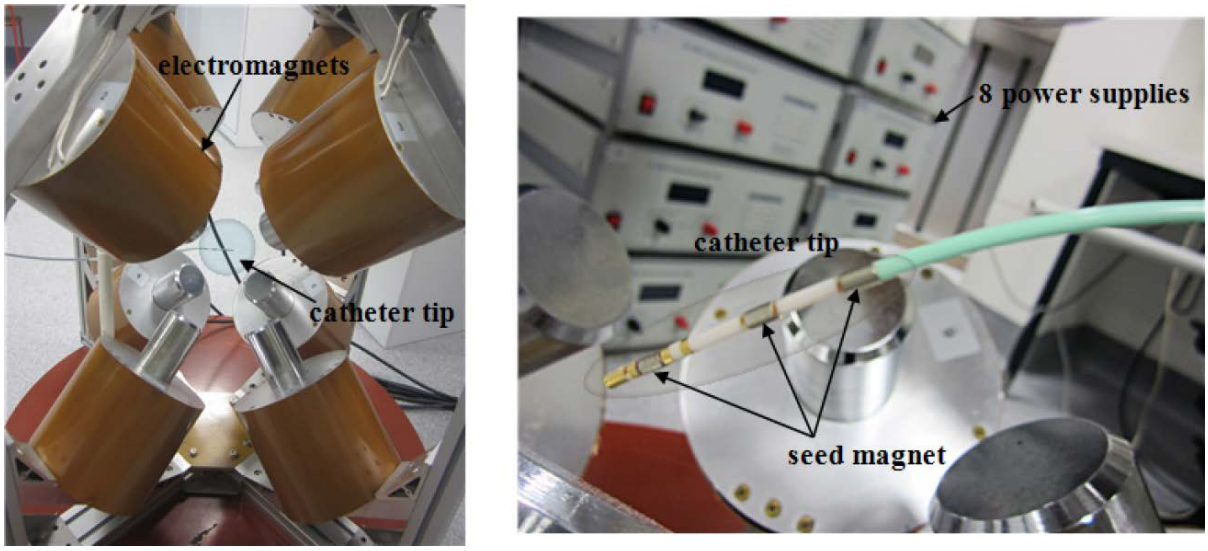

Figure 1.23 Magnetic field generator (MFG) controlling current of multi-electromagnet coils and magnetic steerable catheter for arrhythmia [55]

To apply percutaneous coronary intervention (PCI) procedure, distance between magnet and magnetic field generator have to increase for patient's body [56]. Intensity of magnetic field is inversely proportional to the distance with target position [57]. It is very hard to bend the structure with high bending stiffness using lower magnetic torque [58]. This problem was overcome either to increase size of magnet or to improve performance of magnetic field generator [28, 30, 45, 47, 57]. The former is under many restraints about outer diameter of guidewire (GW) smaller than inner diameter of both catheter and coronary arteries (CA) for percutaneous coronary intervention (PCI) surgery. Eventually, magnetic field generator has to improve the performance. Commercial magnetically actuated guidewires, such as Cronus (Stereotaxis, St Louis, Mo), were manufactured with the big scale permanent magnet and high intensity of magnetic field [56, 59]. When the intensity of magnetic field increase, the required inductance and current of system should increase [57, 60]. Percutaneous coronary intervention (PCI) surgery is demanded fast response for patient's safety due to checking with clinician's eye through image such as vision and radiography [8, 38]. This point induces to be hard the

precisely manipulation caused by phase difference or time delay [61, 62]. Therefore, magnetically actuated guidewire has to be controlled under low torque or force in limitation of geometry instead of increasing intensity of magnetic field. In this research, actuated guidewire is applied mechanical property of polydimethylsiloxane (PDMS) material to manipulate guidewire of tip with low magnetic torque. Pillar structure composed with polydimethylsiloxane (PDMS) is more flexible compare with stiffness of conventional guidewire (GW) and is able to bend with low mechanical force or torque [20]. To manipulate the pillar structure for remote control, the permanent magnet was embedded at the pillar structure [28, 30]. This fabrication process for magnetically actuated pillar structure was applied replica modeling method which is used in micro-electro mechanical system (MEMS) device [63-66]. Characteristics of the fabricated microrobot is biocompatible and flexible. The flexible microrobot was attached at the tip of guidewire (GW) for higher precisely control. Flexible microrobot based on guidewire is helpful at manipulation of guidewire (GW) tip.

II. DESIGN and MECHANSIM

2.1 Medical microrobot based on guidewire (GW)

In this thesis, medical microrobot for treatment of chronic total occlusion (CTO) has been developed. This medical microrobot was attached to guidewire (GW) tip and steered using magnetic torque generated by uniform magnetic field. Remotely controlled flexible microrobot was applied with percutaneous coronary intervention (PCI) procedure. This flexible microrobot was moved to progress toward the desired way in blood vessel using control of external magnetic field (Figure 2.1).

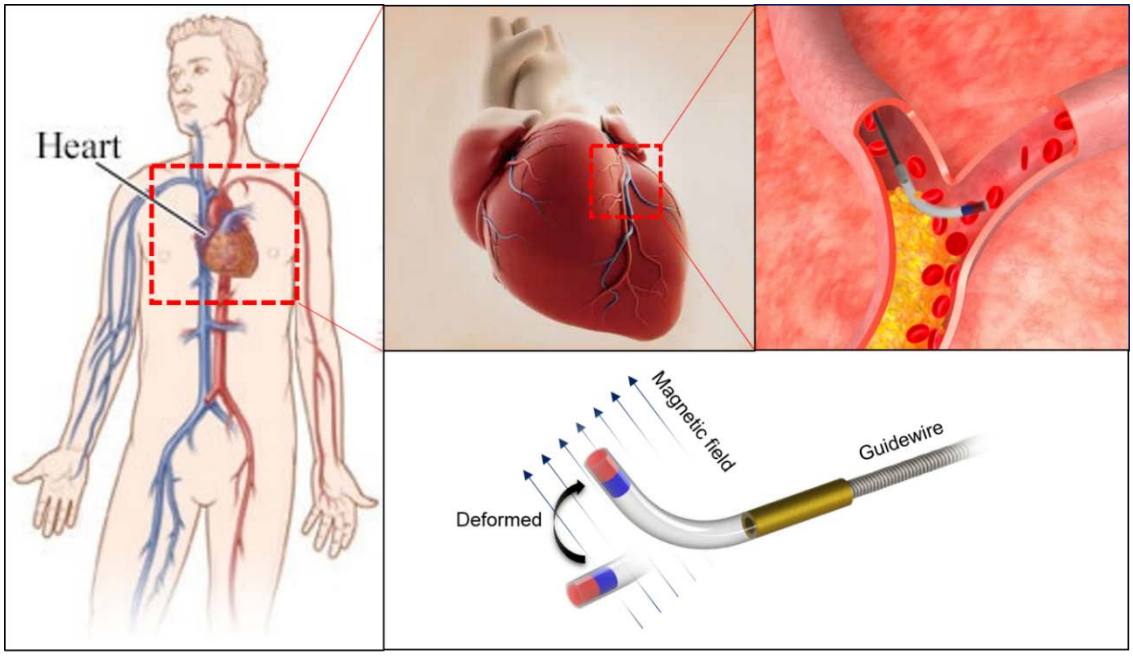

Figure 2.1 Schematics of flexible microrobots attached to tip of guidewire for medical applications

2.2 Mechanism of flexible microrobots.

As previously mentioned, flexible microrobots was steered by adjusting magnitude and direction of magnetic field (Figure 2.2). Magnetically actuated microrobot was applied the simple method which is to use alignment between magnetic agent and external magnetic field such as compass or motor [46]. In uniform magnetic field, the microrobots was applied two torque. One is magnetic torque caused by alignment between the permanent magnet embedded at inside of the microrobot and external magnetic field (Equation (2-1)) [45, 46].

$$\mathrm{T}_{magnetic} = m \times B = \mathrm{mBsin}(\gamma - \theta) \tag{2-1}$$

Where m is magnetization of the permanent magnet, B is magnitude and direction of external magnetic field, γ is direction of external magnetic field, θ is deformation angle of tip of cantilever beam. The other torque is mechanical torque generated by deformation energy. To drive this mechanical torque, this microrobot based on guidewire was assumed as the cantilever beam. Connection between guidewire and microrobot is fixed condition due to differentiations of young's modulus of materials, respectively. permanent magnet embedded microrobot is rigid body with relative to structure compare with polydimethylsiloxane (PDMS) material. This assumed microrobot was able to apply the Euler-Bernoulli equation (Equation (2-2)) [58].

$$\theta = \frac{\mathrm{T}_{mech} L}{EI} \tag{2-2}$$

Where L is length from fixed condition to starting position of permanent magnet, E is young's modulus, I is 2nd moments of inertia of beam. This actuated microrobot is bended until reaching equilibrium state between magnetic and mechanical torque (Equation (2-3)).

$$\mathrm{T}_{magnetic} = T_{mechanical} \tag{2-3}$$

$$\theta = \frac{mBLsin(\gamma-\theta)}{EI} \tag{2-4}$$

$$\gamma = \theta + \sin^{-1}\left(\frac{EI}{mBL}\theta\right) \tag{2-5}$$

Movement of magnetically actuated microrobot was derived using Euler-Bernoulli equation (Equation (2-4), Equation (2-5)). Parameter for actuation of microrobot was dominant direction and intensity of magnetic field and stiffness of beam structure composed with poly-dimethylsiloxane (PDMS) material.

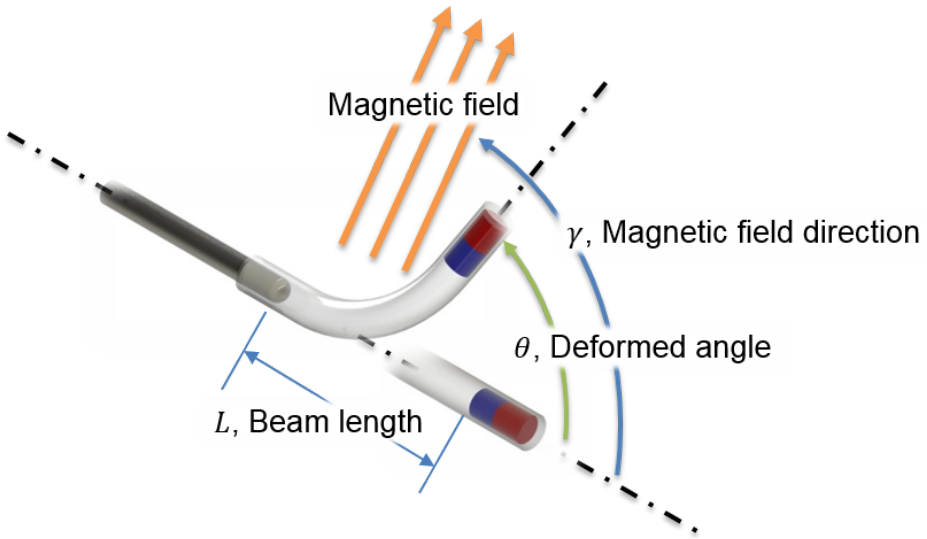

Figure 2.2 Mechanism of flexible microrobot using magnetic actuation

2.3 Design of flexible microrobots based on guidewire (GW)

The flexible microrobots were designed, considering about four points for medical application. One is that diameter of flexible microrobots have to be sufficiently smaller than of coronary arteries. Second is to be actuated by magnetic field with low intensity because of limitation of intensity of uniform magnetic field generated by electromagnetic coil system. Third is the connecting method between flexible microrobots and guidewire. Lastly, surface of flexible microrobots has to be biocompatible.

To control with magnetic torque generated by uniform magnetic field, the microrobots have to include magnetic agent such as the permanent magnet (NdFeB). Flexible microrobots was fabricated by elastomer with low young's modulus to be actuated low intensity of magnetic field which is under 15 mill-tesla. Microrobots have the brass pipe because the brass is non-magnetic material to remove influence of external magnetic field. This brass pipe is connector between flexible microrobot and guidewire with 0.014-inch diameter. Shape of flexible microrobots was designed as cylindrical shape to be steered freely in a vertical axis direction of body axis with long length.

Table 1. Geometry parameter of flexible microrobots

	Geometry Parameter, Diameter × Length [㎛]
PDMS	Ø500 × 3000, Ø500 × 6000
NdFeB, N52	Ø400 × 800
Brass Pipe	O.D 500 × I.D 300 × 2000
Microspring	Size: Ø500 × 2000, Wire: Ø60 × 66 turn
Guidewire	Ø340 (0.014 inch)

III. FABRICATION

3.1 Fabrication of Metal and PDMS mold for replica molding method

3.1.1 Wire-cutting manufactured metal mold

Flexible microrobots were fabricated by replica molding method [63, 67]. For replica molding method, design of master molds was divided into two parts which are a male part and a female part. Two parts include semicircular type hole with 0.5 mm diameter and 15 mm length. (Figure 3.1) Master molds were manufactured by wire electric discharge machining with stainless steel (Figure A.1).

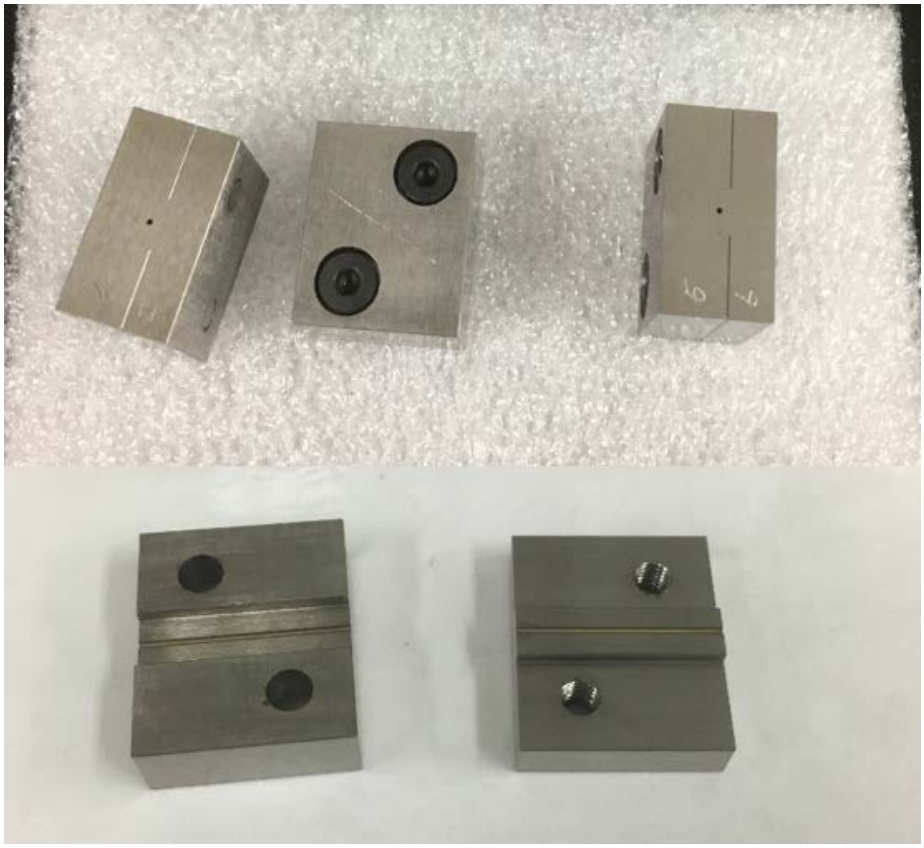

Figure 3.1 Fabricated metal mold using wire-cutting machining; (Above) combined pair of mold. (Below) pair of mold

3.1.2 Fabrication of PDMS mold using hydrophilic coating and surface treatment

Polydimethylsiloxane (PDMS) mold has several advantage than metal mold with stainless steel. One is that polydimethylsiloxane (PDMS) is optical transparent material [66]. Transparency is able to confirm formation of flexible microrobots. Other advantage is that fabricated microrobots in polydimethylsiloxane (PDMS) mold is more flexible than fabricated microrobots in metal mold with stainless steel because heat transfer coefficient of stainless steel is higher than heat transfer coefficient of polydimethylsiloxane (PDMS).

In the research, polydimethylsiloxane (PDMS) mold were fabricated by replica molding method using master mold with stainless steel. Fabrication process is as followed. First of all, base and cured agent of polydimethylsiloxane (PDMS) was mixed in the weight rate of ten to one. A small quantity of methyl blue solution was added at the mixture of polydimethylsiloxane (PDMS) for separation between casting mold and transparent mold. Master molds composed stainless steel were cleaned with acetone, isopropyl alcohol (IPA), and deionized water. Cleaned master molds fixed in petri dish. Colored polydimethylsiloxane (PDMS) mixture was poured on the petri dish (Figure 3.3). Next step, the filled petri dish was degassed for one hours in vacuum chamber and cured at the 80 Celsius degree for 2 hours in oven (JSOF-100, JSR, KOREA). Casting mold with polydimethylsiloxane (PDMS) was released from petri dish and master mold composed with stainless steel. Casting mold required surface treatment for connection between casting mold and transparent mold due to using same material which is polydimethylsiloxane (PDMS). Cured casting molds were conducted for hydrophilic coating using oxygen plasma equipment (Plasma equipment(Air), CUTE, FEMTO SCIENCE) [68]. Condition of plasma equipment is 75 sccm of amount of gas, 65 W of bias power and 30 sec of operating time. After hydrophilic coating, surface of casting molds was coated trichloro (1H,

1H, 2H, 2H-perfluorooclyl)-Si (Sigma-Aldrich) using vacuum evaporation to be prevent combination of structure composed with same material which is polydimethylsiloxane (PDMS) [69]. Transparent molds were fabricated by same fabrication process, which is above mentioned negative mold method, using the casting mold with surface treatment (Figure 3.2).

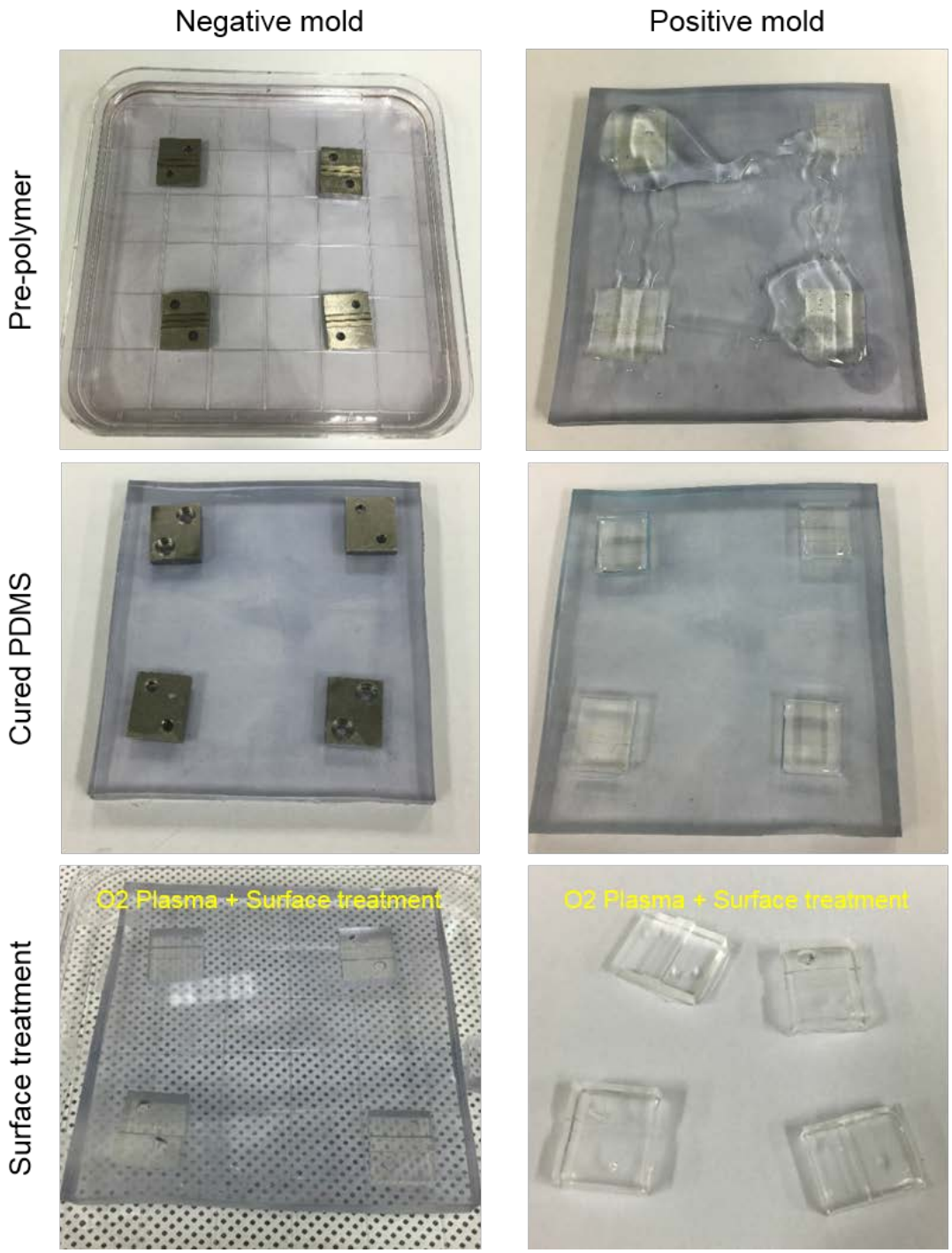

Figure 3.2 Fabrication process of PDMS mold

3.2 Fabrication of flexible microrobot

Flexible microrobots were fabricated by negative mold method using transparent mold. the permanent magnet (NdFeB, N52, China Neodymium Magnet Manufacturer, China) and brass pipe were placed on a male part of transparent mold (Figure 3.3-a). In next step, a male part with positioned permanent magnet and brass pipe was combined a female part. The combined mold was attached the big permanent magnet on the one side to control position of magnet inserted in combined mold and fixed in container (Figure 3.3-b). Colored polydimethylsiloxane (PDMS) mixture is that base and cured agent was mixed in weight rate of ten to one and methylene blue solution was mixed in rate with two hundred microliters per one gram of weight of mixed polydimethylsiloxane (PDMS). The colored polydimethylsiloxane (PDMS) mixture was poured in the prepared container with combined mold for degassing and curing process. To fill pre-polymer of colored polydimethylsiloxane (PDMS) mixture toward hole of combined polydimethylsiloxane (PDMS) mold, container was degassed for one hours in the vacuum chamber (Figure 3.3-c). After confirmation of removal of bubble in the cylindrical hole of polydimethylsiloxane (PDMS) mold, container with combined mold was cured at the 80 Celsius degree for 2 hours in oven (JSOF-100, JSR, KOREA) (Figure 3.3-d). Flexible microrobots was released from polydimethylsiloxane (PDMS) mold (Figure 3.3-e).

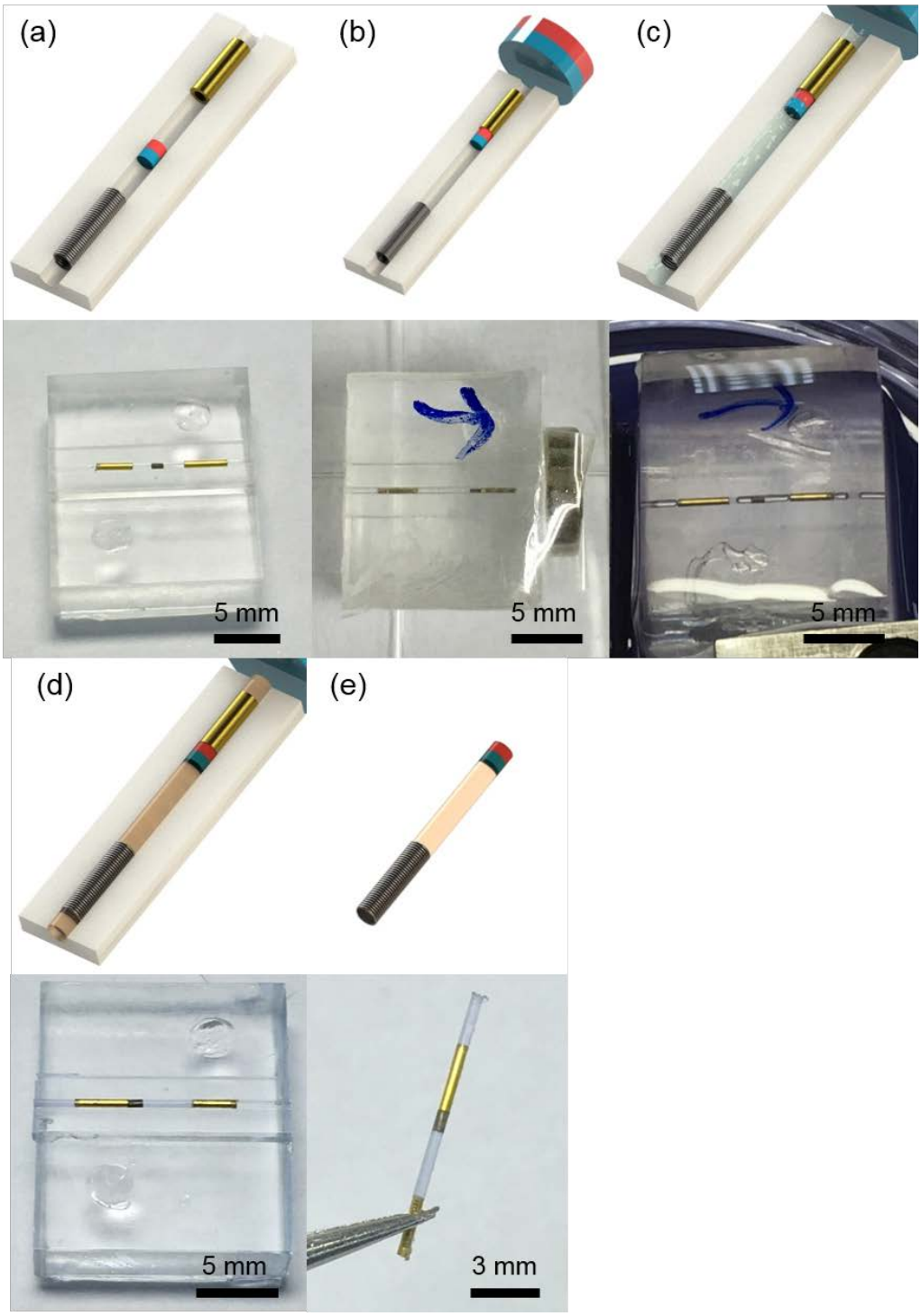

Figure 3.3 Fabrication process of flexible microrobots using replica molding method and PDMS; (a) adjusting length of microrobot using gap measured by micrometer. (b) moving the magnet using approach of big magnet. (c) Poured the pre-polymer in Petri dish and degassed in vacuum chamber for 1 hours. (d) Cured in the oven at the 80℃ for 2 hours. (e) Successfully fabricated flexible microrobot.

IV. EXPERIMENTS

4.1 Multiphysics modeling of flexible microrobots for FEM analysis

In research, flexible microrobots are composed with soft material which is polydimethylsiloxane (PDMS) and the permanent magnet which is neodymium magnet (NdFeB, N52, China Neodymium Magnet Manufacturer, China). Nonlinear and multi-physics simulation of flexible microrobots under external magnetic field was conducted using commercial finite element method (FEM) software (COMSOL Multiphysics 5.25a, COMSOL Inc., North America).

4.1.1 Geometry and material property of multiphysics modeling

Domain of two dimensional (2D) multiphysic modeling of flexible microrobots consist of the permanent magnet, polydimethylsiloxane (PDMS), working space with air, and infinite element domain on outermost space (Figure 4.1). Geometry of permanent magnet of multiphysics modeling has 0.4mm of width, 0.4mm of height, and 0.8mm of length (Table 1). Geometry composed with polydimethylsiloxane (PDMS) has not circle cross-section with 0.5mm of diameter but rectangular cross-section with 0.4mm of width and 0.5mm of height for two dimensional (2D) analysis (Table 1). The permanent magnet was located at one side of structure composed with polydimethylsiloxane (PDMS). Domain of surrounded microrobots for formation of magnetic field in the air has 30 mm of width and height. Outermost domain is infinite element domain which is able to reduce unnecessary mesh. Several domains were filled by information of mechanical and magnetic property (Table 2).

Table 2. Material property of flexible microrobots using FEM analysis

Material	**Polydimethylsiloxane (PDMS)**	**Neodymium magnet (NdFeB, N52)**
Density	970 kg/m^3	7500 kg/m^3
Young's modulus	750 kPa	160 GPa
Poisson's ratio	0.49	0.24
Relative permeability	1	1.05
Remanent flux density		1.43T

4.1.2 Boundary conditions (B.C) of multiphysics modeling

Boundary condition of multiphysics modeling of flexible microrobot were largely divided by three parts (Figure 4.1). Domain of the permanent magnet was applied by Maxwell surface stress tensor in boundary load of structure module for external magnetic torque and force. Domain of polydimethylsiloxane (PDMS) beam structure has fixed boundary condition (B.C) which is unable to generate displacement. Remained boundary in polydimethylsiloxane (PDMS) beam was applied prescribed mesh displacement condition to be moved mesh of contacted surface between polydimethylsiloxane (PDMS) and the other material such as air and magnet according to deformation of flexible microrobot due to magnetic torque. boundary of secondary larger spare has boundary condition for formation of external magnetic field.

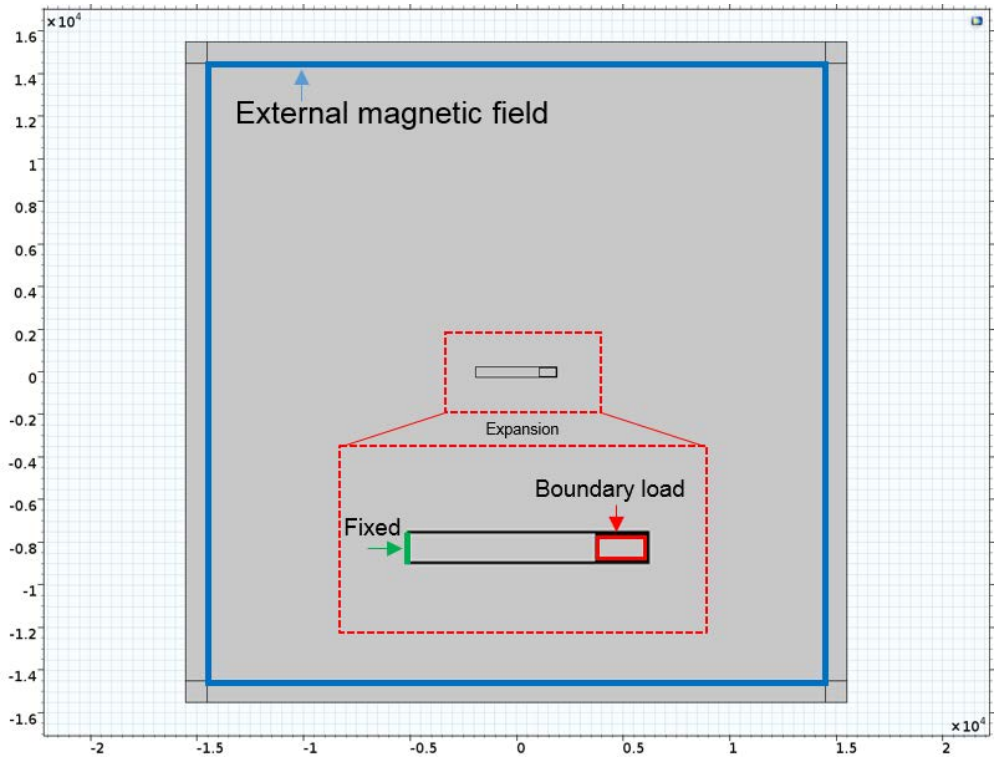

Figure 4.1 Geometry and boundary condition of two dimensional (2D) multiphysic modeling of flexible microrobot

4.1.3 Parameter for analysis of multiphysics modeling

Flexible microrobot was assumed as magnetically actuated cantilever beam. Deformed angle of flexible microrobot under external magnetic field was effected by length of microrobot, intensity of magnetic field, and direction of magnetic field. In this research, flexible microrobot was simulated to obtain deformed angle of flexible microrobot according to variable parameter using finite element method (FEM) analysis (Table 3).

Table 3. Parameter for simulation of flexible microrobot

Parameter	Value
Length of flexible microrobots	3000 [㎛]
Direction of magnetic field	From 0 to 170 [deg]
Intensity of magnetic field	5, 10, 15 [mT]

4.2 Experimental environments

4.2.1 Magnetic field generator

The fabricated flexible microrobot based on guidewire was actuated according to external magnetic field. To control microrobot, external magnetic field is uniform in the constant space. Magnetic field generator (Minimag, Aeon Scientific GmbH, Switzerland) was used at the experiment of flexible microrobot for formation of uniform magnetic field [50]. This magnetic field generator consists of part for electromagnetic coils, electro circuit system, and control system. Electromagnetic coils of magnetic field generator were eight of solenoid type coil. Geometry of solenoid type coils was divided by two groups which has four coils and arranged at intervals of 90 degrees. Two groups of electromagnetic coils are roughly arranged at minus 64 degrees and minus 45 degrees with relative to horizontal angle of structure of magnetic field generator [50]. Half sphere type electromagnetic coil system was generated magnetic field and gradient magnetic field through the entering current control at each coils. This generated magnetic field has spherical space with one mill-meter of diameter to be uniform intensity and direction of magnetic field.

4.2.2 Steering experiment of flexible microrobots under external magnetic field

To obtain characterization of flexible microrobots, deformed angle of flexible microrobot were measured under external magnetic field. The micro pipe makes of brass and has 1.2 mm of outer-diameter and 0.5 mm of inner-diameter. One end of brass micro pipe was located toward center on the magnetic field generator for settling flexible microrobot (Figure 4.2). Movement of flexible microrobot was measured by imaging lens (VZM 600i Zoom Imaging Lens, Edmund Optics Inc., USA) and charge-coupled device (CCD) camera (Grasshopper, Point Gray Research, Inc., Canada). To be captured three dimensional (3D) movement of flexible microrobot under magnetic field, both imaging lens and charge-coupled device (CCD) camera were relatively arranged for the top and side view. These experiments were conducted by adjusting variable parameter (Table 4). The captured images of deformed angle of flexible microrobots were quantified toward numerical value using protractor.

Table 4. Parameter for steering experiment of flexible microrobot

Parameter	Value
Length of flexible microrobots	3000, 6000 [㎛]
Direction of magnetic field	0, 30, 60, 90, 120, 150, 170 [deg]
Intensity of magnetic field	5, 10, 15 [mT]

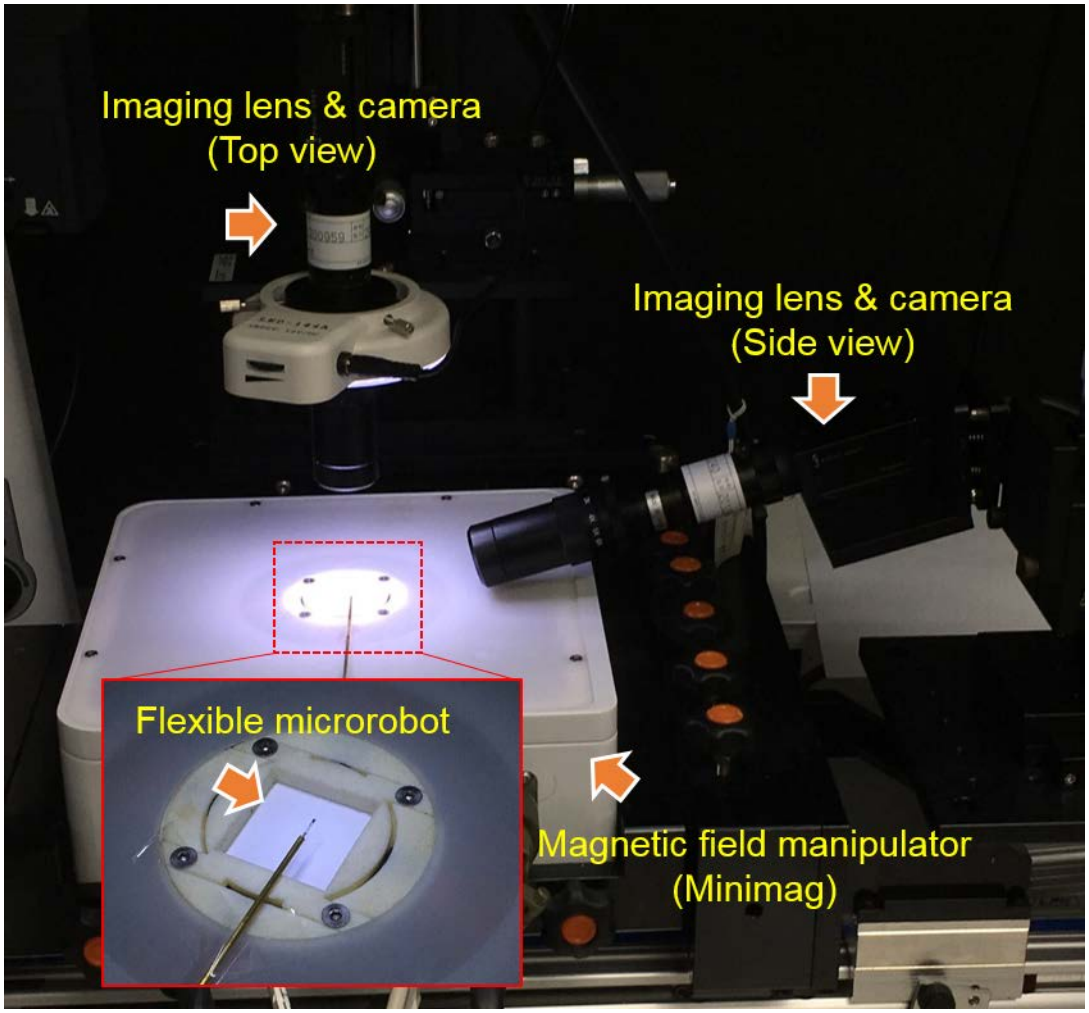

Figure 4.2 Steering test of flexible microrobots in the air

4.2.3 *In vitro* experiments in branch and vascular networks model

Purpose of flexible microrobots based on guidewire (GW) is to substitute manually controlled method of guidewire for guiding toward the position of lesion. This experiments is to prove possibility of movement along the desired path in blood-vessel phantom with one or more branches using magnetically steerable microrobots. The blood-vessel phantoms were printed by three dimensional (3D) printer (Projet 3500, 3D Systems, US). Blood vessel phantoms with one branch were designed to get the variable branch angle which consist of 15, 30, 45, 60, 75, and 90 degrees. Blood-vessel networks phantom has multi branch for mimic coronary arteries in two dimensional (2D) plane (Figure 4.3). Transparent plate was inserted at the window of printed blood-vessel phantoms and combined using epoxy. Guiding catheter was inserted in the inlet of the blood-vessel phantom in order that *in vitro* experimental environment is similar to surgical environment using percutaneous coronary intervention. Fabricated blood-vessel phantom was placed on the magnetic field manipulator for magnetic actuation of flexible microrobots and filled by the mixture with deionized (DI) water and surfactant for reduction of surface friction between flexible microrobots and blood-vessel phantom (Figure 4.4). flexible microrobots were attached to tip of guidewire (GW) and inserted until entrance of branch along the inner pathway of guiding catheter. This microrobot was steered toward the wanted direction by adjusting uniform magnetic field which is generated by magnetic field manipulator and moved by manually pushing and pulling using operator’s hand.

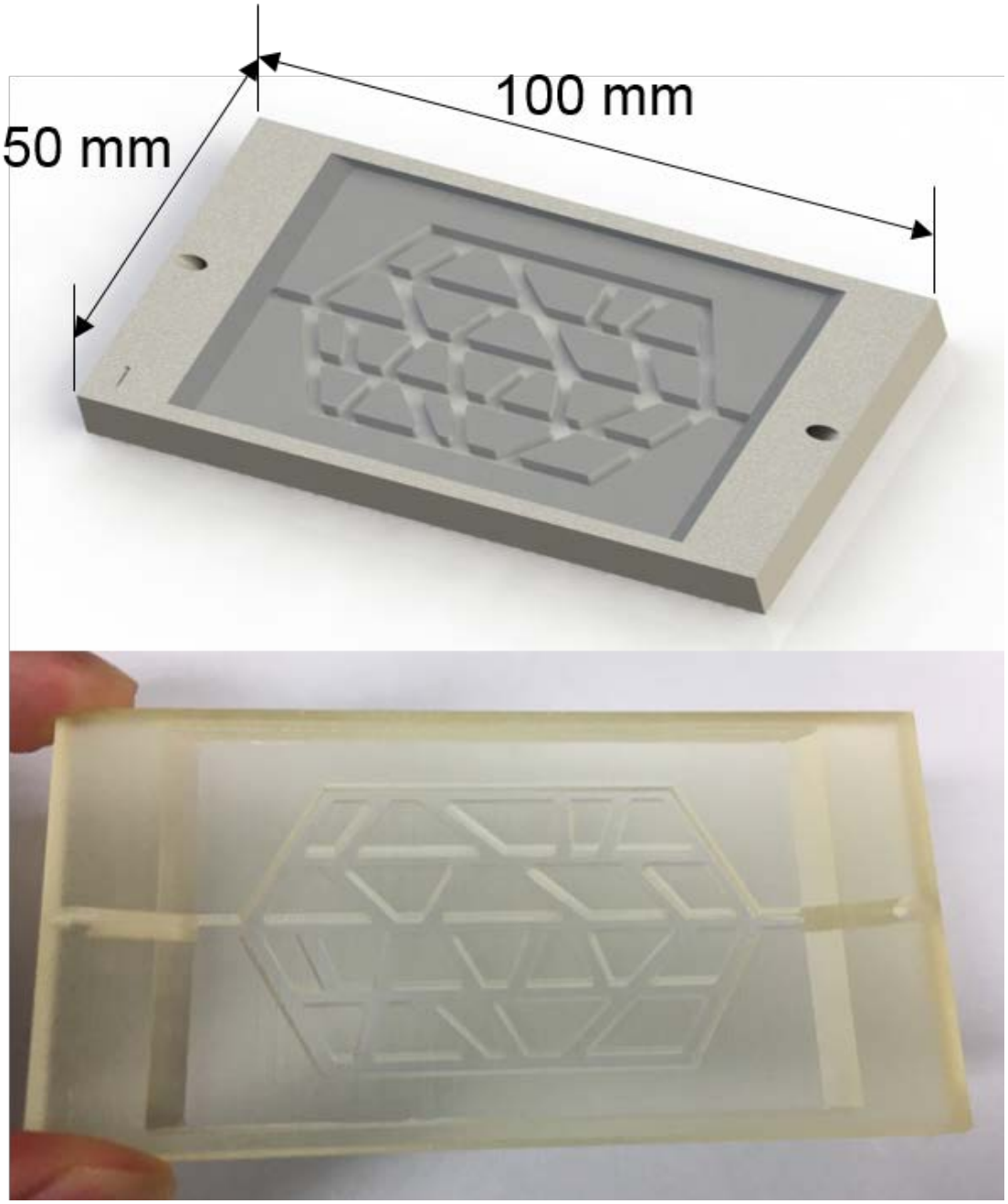

Figure 4.3 Rendering image and 3D printed structure of vascular network model fabricated by three dimensional (3D) printer.

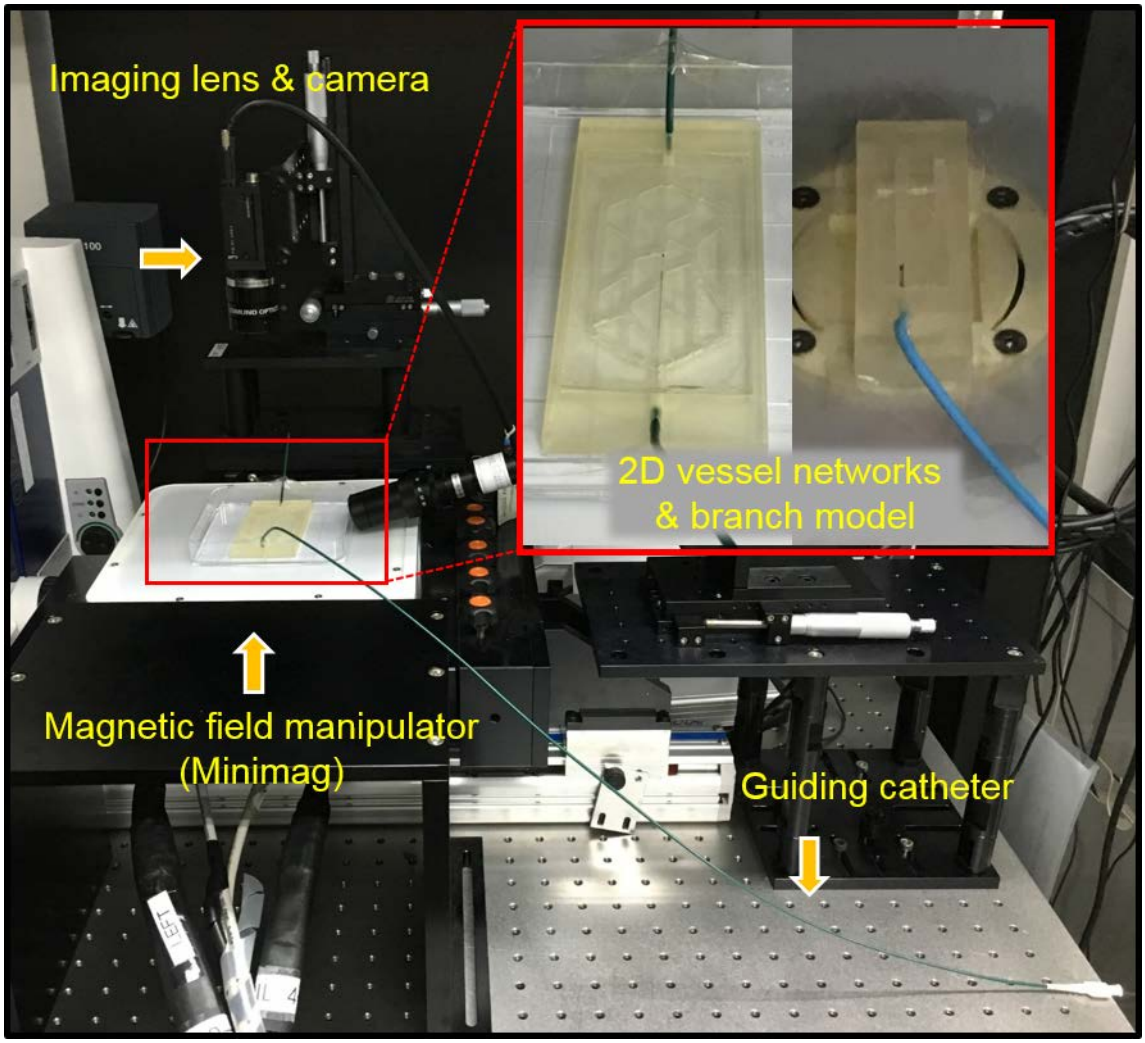

Figure 4.4 Tracking test in vascular branch model

V. RESULTS

5.1 FEM result of flexible microrobots using multi-physics modeling

Flexible microrobots was simulated to confirm magnetic actuation of structure composed with soft material. Result of simulation of flexible microrobots was shown magnetic field, deformed angle, and mesh shape (Figure 5.1). Blue line is mesh shape of multiphysics modeling. This mesh was chased around changed boundary of structure due to movement of deformed flexible microrobots. Red arrow is vector of magnetic field generated at around microrobot. Big red arrow which place on the magnet domain is always head for long-axis of magnet by changing direction of external magnetic field. Small red arrows which is far away at structure have same vector of magnetic field. Deformed angle of flexible microrobot is 13 degrees under magnetic field with 5 mT of intensity and 30 deg of direction with relative to X-axis. Maximum deformation angle of flexible microrobot under magnetic field with 5mT is measured 29 degrees at the 120 degrees of magnetic field direction.

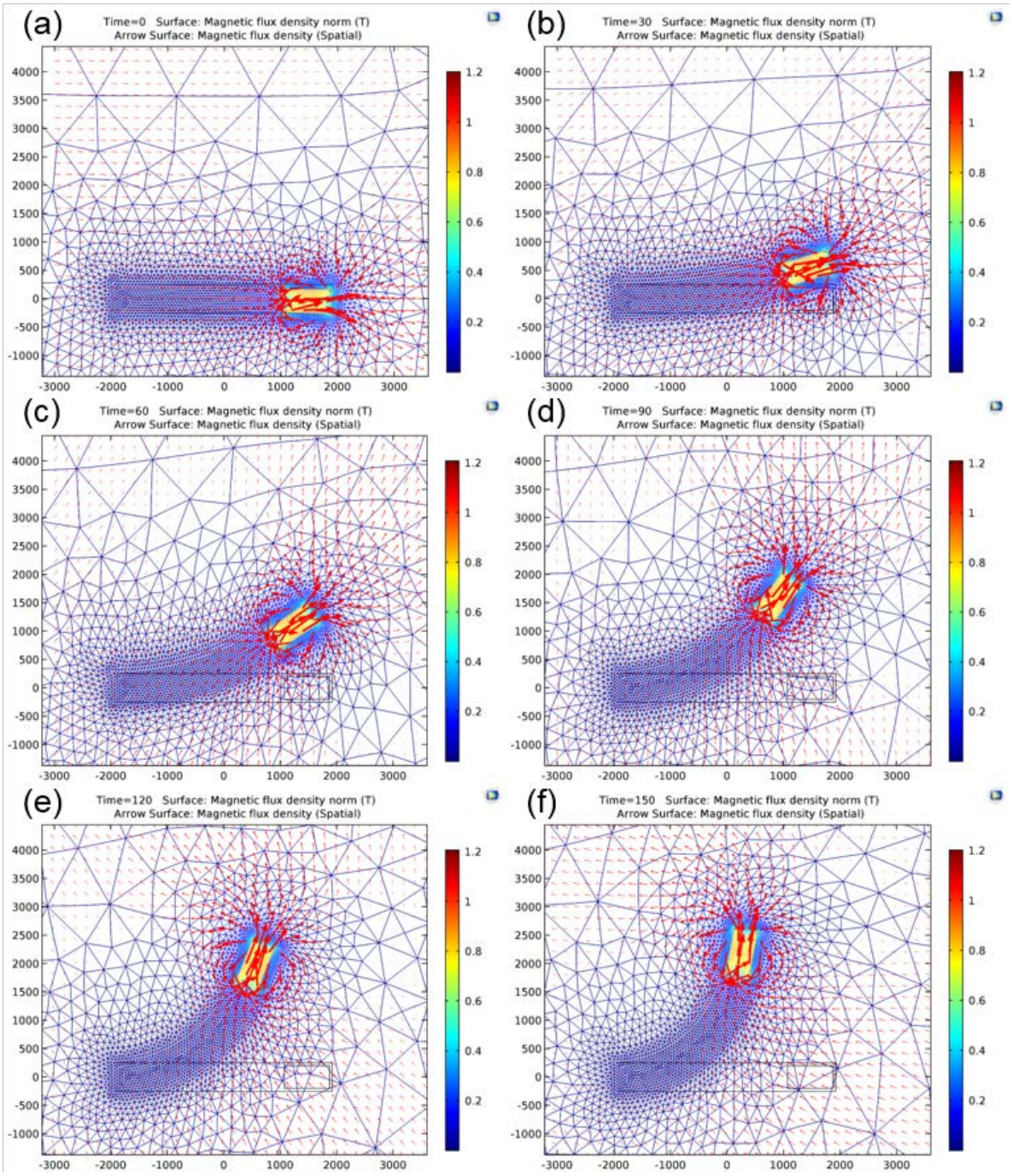

Figure 5.1 FEM simulation result of flexible microrobot under uniform magnetic field with 15mT of intensity from 0 to 150 degree of direction; mesh (Line) and property of magnetic field (Arrow)

To be confirm mechanism, torque applied at magnet was extracted in simulation of multiphysics modeling (Figure 5.2). along changing direction of magnetic field from 0 deg to 150 deg.

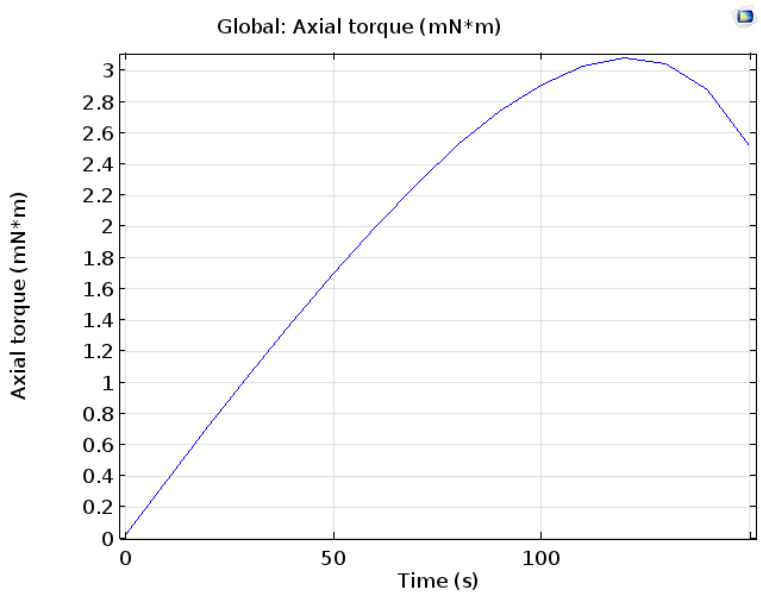

Figure 5.2 Characterization of magnetic torque of the permanent magnet in flexible microrobots according to direction of magnetic field.

Simulation of flexible microrobots compared to experimental imaging result (Figure 5.3). Under external magnetic field with 15mT of intensity and 90 deg of direction with relative to X-axis, deformation angle of multiphysics modeling of flexible microrobots was simulated 75.6 deg. and experimental deformation angle of flexible microrobot was measured 78.9 deg.

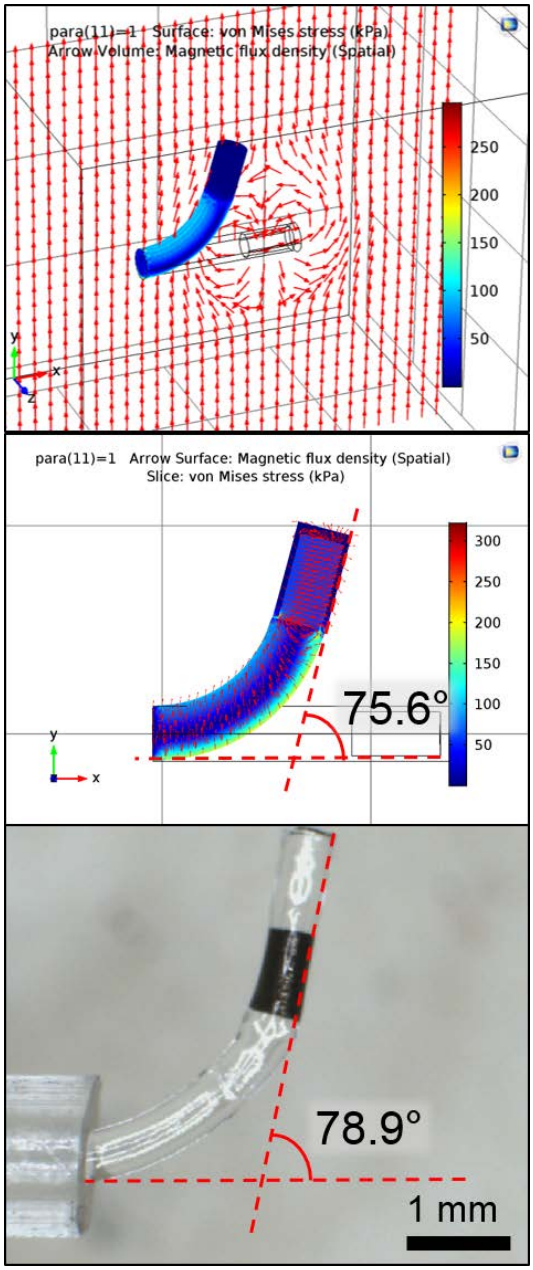

Figure 5.3 COMSOL simulation result

5.2 Steering function of magnetically actuated flexible microrobots

5.2.1 Three dimensional (3D) movement of flexible microrobot

Flexible microrobots were steered in the air under external magnetic field generated by magnetic manipulator which is Minimag. Flexible microrobots is possible to be deformed at each direction according to direction of magnetic field. This image of deformed microrobots were obtained as condition of magnetic field with 15 mill-tesla of intensity and 0 degrees, 120 degrees in XY plane, and 90 degrees in XZ plane of direction with relative to X-axis which is initial condition of static position of flexible microrobot (Figure 5.4 (a-c).

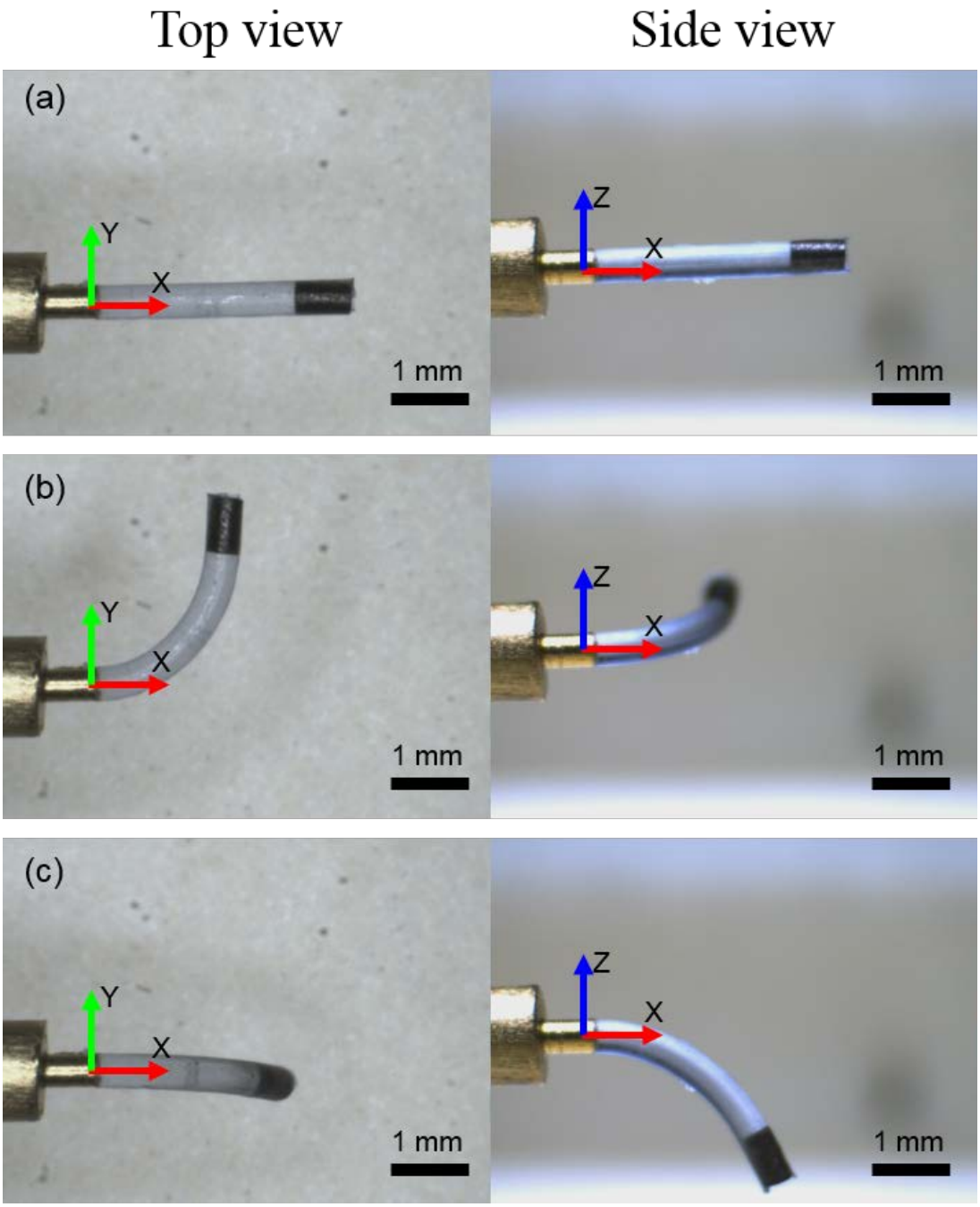

Figure 5.4 Captured image of flexible microrobot under magnetic field with 15mT of intensity; (a) direction which is parallel to X-axis. (b) 120 deg of direction with relative to X-axis in XY plane. (c) 90 deg of direction with relative to X-axis in XZ plane

5.2.2 Characterization of flexible microrobot

This graphs were characterized relationship between magnetic field and deformation angle of flexible microrobots with 3.8 mm of total length (Figure 5.5-7). Applied magnetic field is 5 mT of intensity and several directions which has range from 0 deg to 170 deg. Black line is experimental data obtained through steering experiments of flexible microrobots. Red line is analytic solution using MATLAB (MATLAB 2012b, Mathworks) through the equation derived by Euler-Bernoulli Beam theory (Equation 2-4, Figure A.2). Blue line was obtained from finite element method (FEM) results of multiphysics modeling of flexible microrobot.

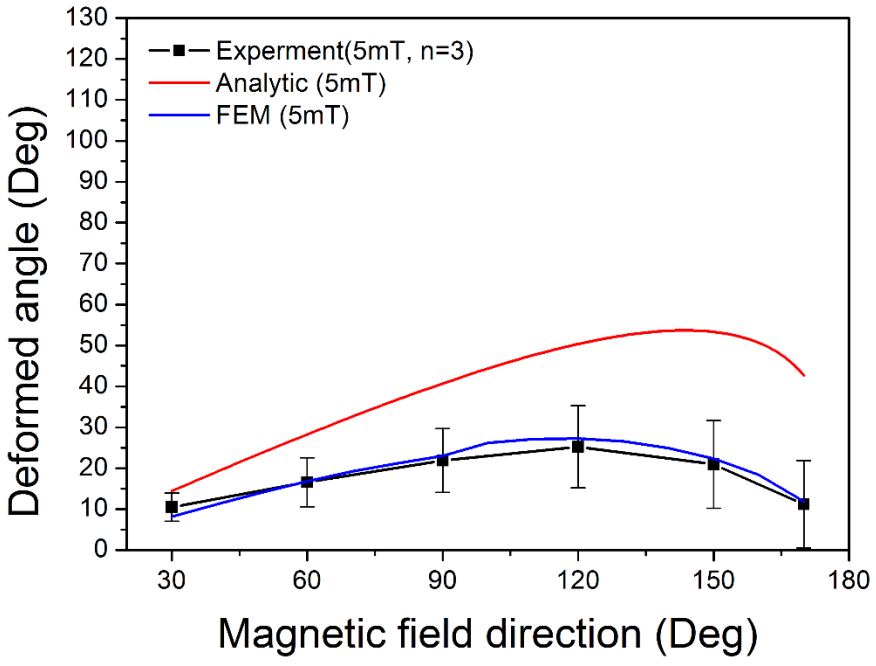

Figure 5.5 Graph between magnetic field with 5 mT and deformation angle

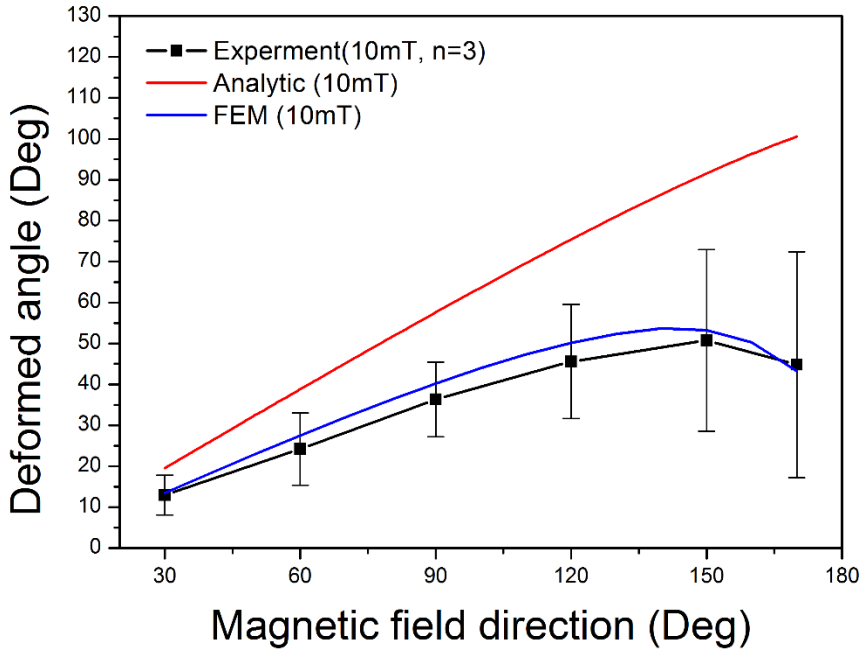

Figure 5.6 Graph between magnetic field with 10 mT and deformation angle

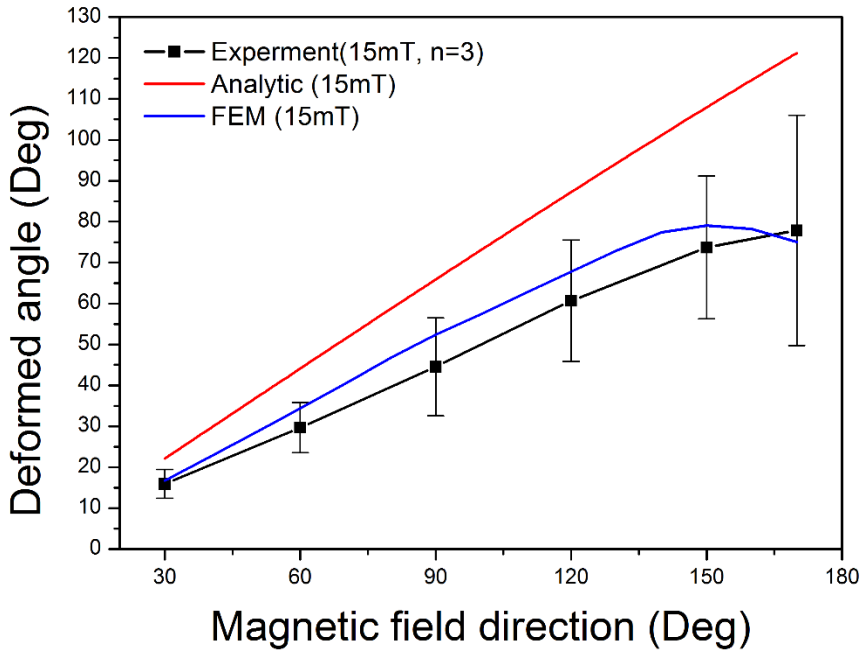

Figure 5.7 Graph between magnetic field with 15 mT and deformation angle

5.3 Track-ability of flexible microrobots

5.3.1 Tracking function of flexible microrobots in single branch phantom

Tracking function of flexible microrobots based on guidewire is very important. This experiments were conducted in single branch phantom using external magnetic field to be confirmed track-ability of flexible microrobots.

Head of flexible microrobots with 3.8 mm of length were steered and tracked toward the wanted path in printed model with 30 degrees of branch angle (Figure 5.8). Under external magnetic field with 15 mT of intensity and almost 10 degrees of direction, guidewire connected flexible microrobot was pushed by operator's hand. In this case, flexible microrobots was moved toward straight. To move toward the bended path, direction of magnetic field was manipulated from 10 degrees to minus 30 degrees. Flexible microrobot with pushing force was moved toward the bended path.

Secondary experiment was conducted in printed phantom the higher branch angle which is 60 degrees. Used flexible microrobot was 7 mm of length and was attached to core wire of guidewire which is more flexible (Figure 5.9). To enter the branch, direction of magnetic field with 15mT of intensity was controlled to minus 70 degrees which is higher than the branch angle. In mid-point, direction of magnetic field was manipulated to minus 40 degrees to be attached upper surface. After this process, flexible microrobot was successfully tracked along the path with 60 degrees of branch angle.

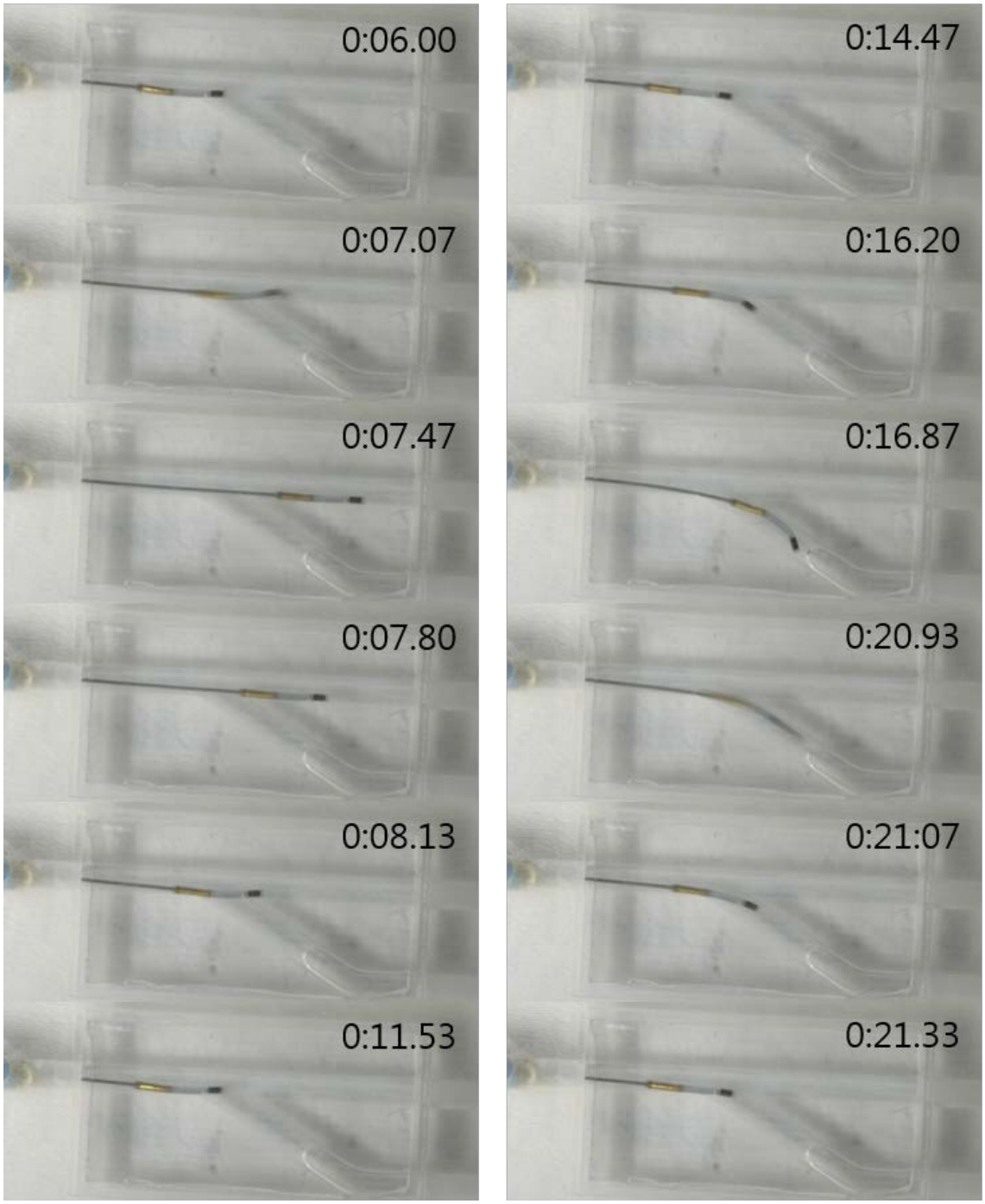

Figure 5.8 Tracking in the branch model with 30 degrees; (Left column) straight. (Right column) Curve.

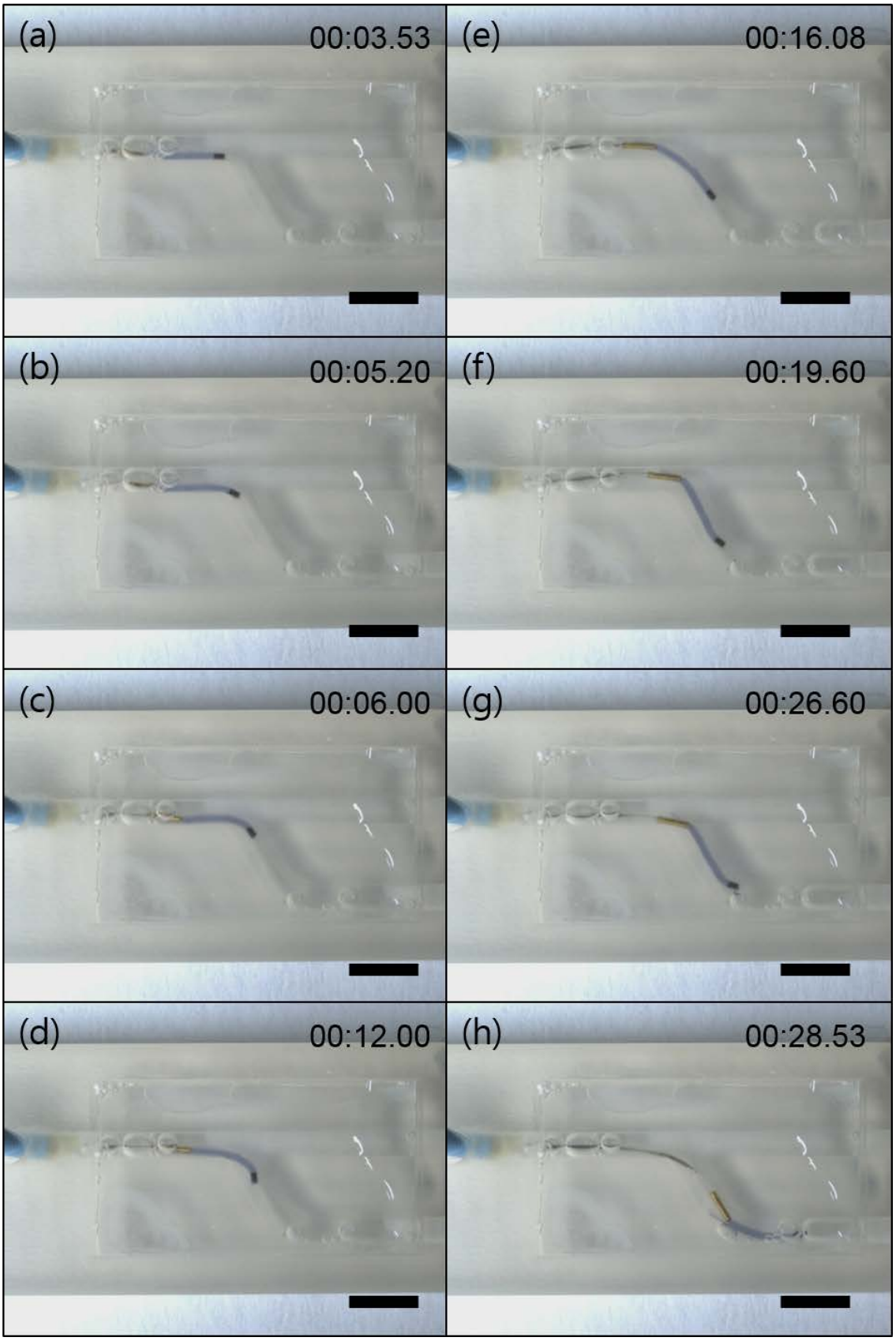

Figure 5.9 Tracking in the branch model with 60 degrees

5.3.2 Tracking function of flexible microrobots in blood vessel network phantom

Track-ability of flexible microrobot was confirmed to be moved until 60 degrees of branch angel in single branch model through above experiments. In this experiments, tracking experiments of flexible microrobot was conducted in the multi-branch model or blood vessel network model. Flexible microrobot attached at guidewire tip was steered by adjusting direction of magnetic field and moved along the wanted path with push and pull by operator's hand (Figure 5.10 (a-c)). The printed model was replaced on magnetic field generator in order to locate head of flexible microrobot in the working space due to limitation of size of working space which has sphere with 1 mm diameter and is generated uniform magnetic field (Figure 5.10 (c-e)). In rear of blood-vessel network model, flexible microrobot was manipulated by changing external magnetic field and pushing with operator's hand (Figure 5.10 (e-h)).

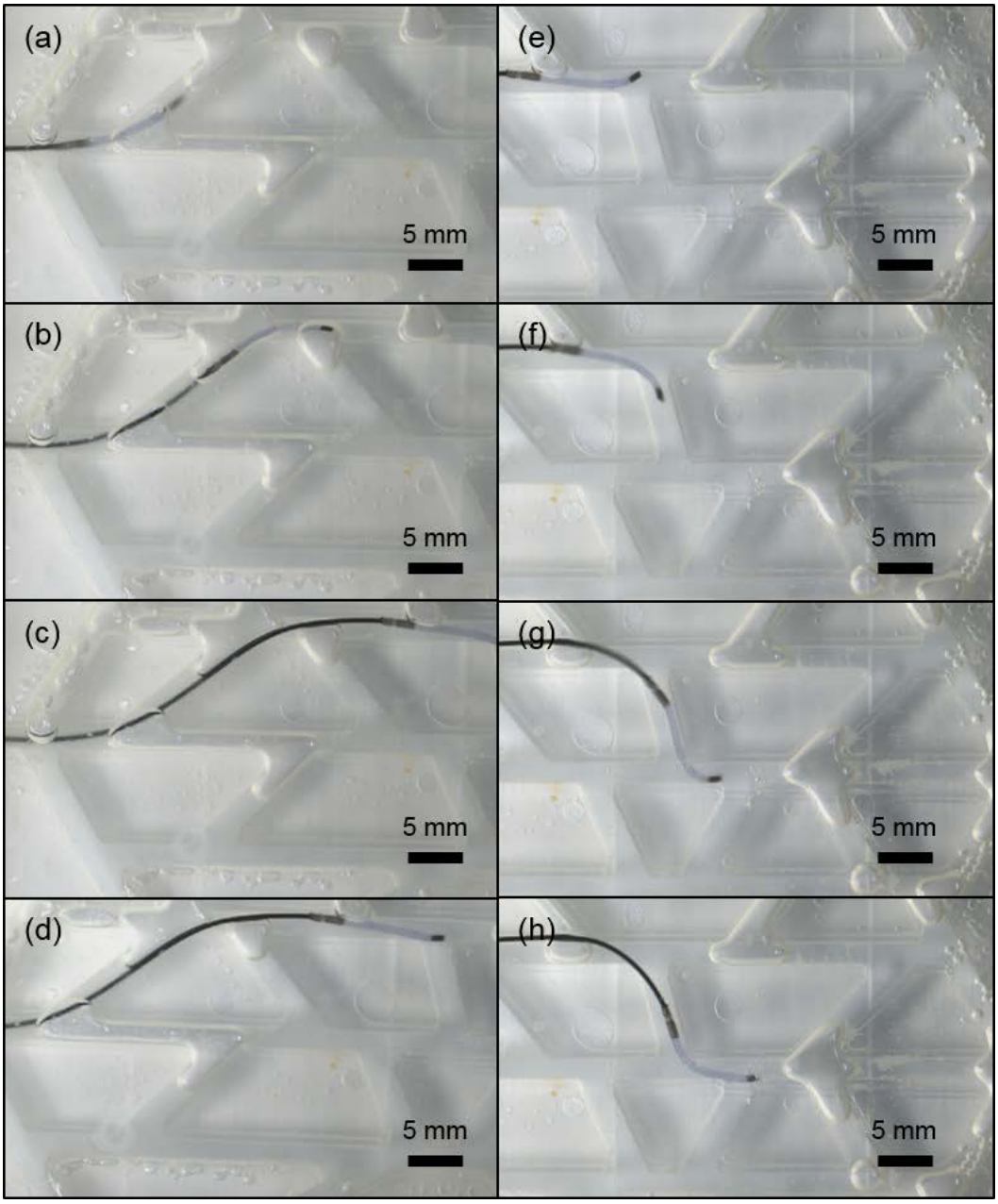

Figure 5.10 Tracking using flexible microrobot in blood-vessel network phantom using Minimag and operator's hand; (a-c) selection at the first branch point. (c-e) moving camera view point. (e-h) selection at the second branch point.

5.4 A robotic assisted percutaneous coronary intervention procedure

5.4.1 Integrated system for robotic assisted PCI procedure

As previous two experiments, characterization of flexible microrobot has steerability and trackability (Figure 5.11 (a)). However flexible microrobot based on guidewire (GW) was unable to progress forward because of absence of degree of freedom about axial direction. For completed remote control, master/slave system (Hanyang University, South Korea) was used to move forward and backward instead of operator's hand [70]. Flexible microrobot based on guidewire (GW) was steered by adjusting direction and strength of external magnetic field which is generated by Octomag and manipulated by pushing and pulling with master/slave system (Figure 5.11 (b, c)) [51].

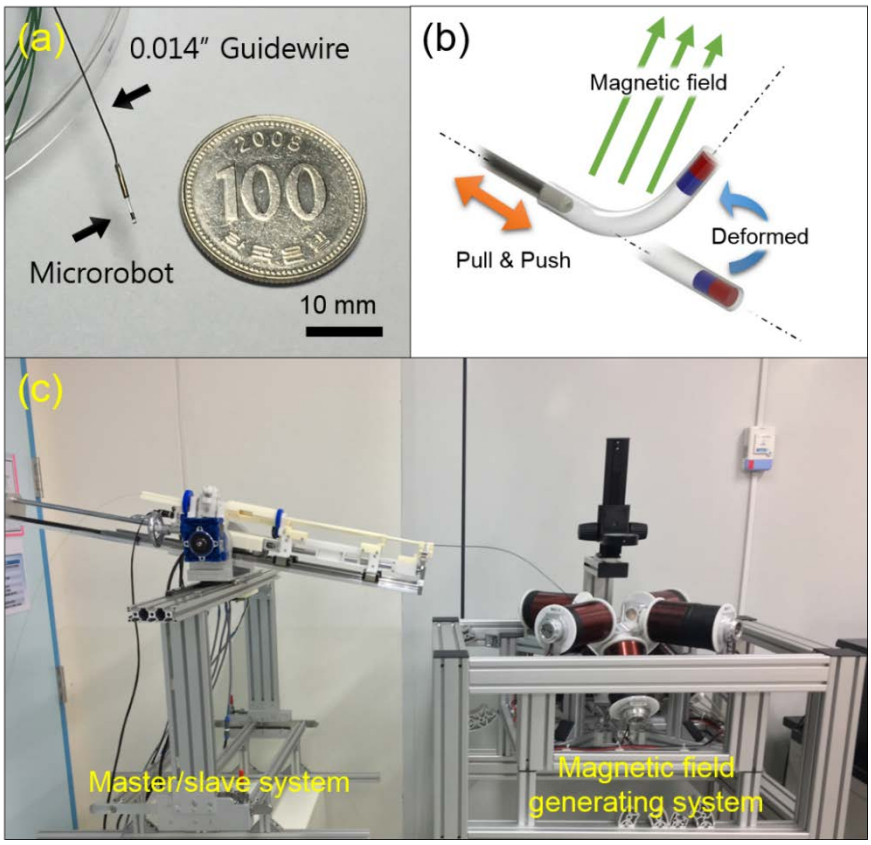

Figure 5.11 Master/slave system for robotic catheterization; (a) compared with a hundred-won coin and flexible microrobot attached guidewire (GW). (b) schematic of controlled flexible microrobt based on guidewire (GW). (c) master/slave system and magnetic field generating system.

5.4.2 *In vitro* experiment with flexible microrobot and integrated system

Flexible microrobot based on guidewire was moved along the fixed guiding catheter at the entrance of phantom using master/slave system. At the branch point, microrobot was bended by controlling external magnetic field which is generated by Octomag and gone forward due to movement of guidewire (GW) by master/slave system (Figure 5.12 (a-c)). Using same procedure at the another branch point, microrobot was finally reaching the desired point (Figure 5.12 (d-f)).

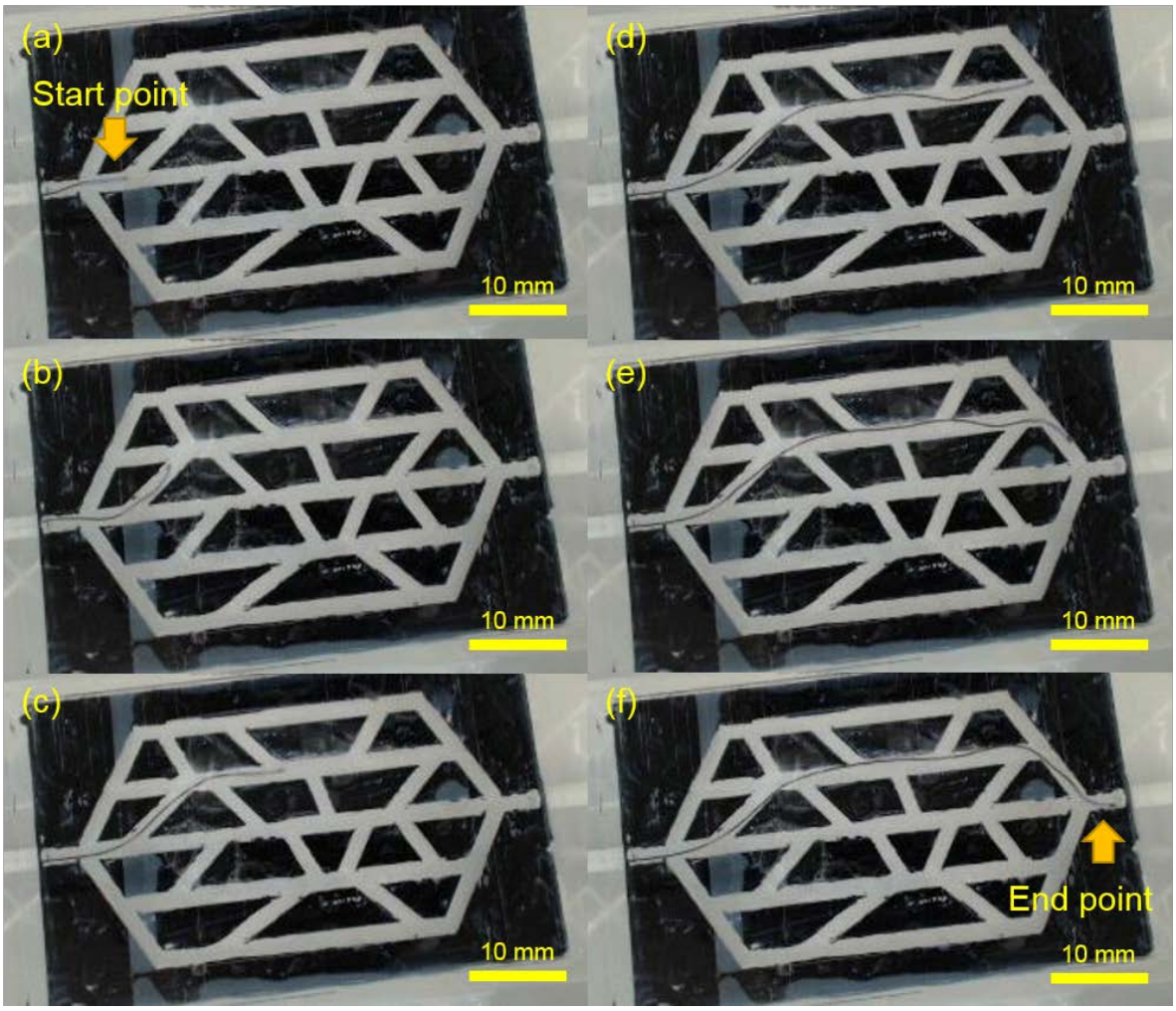

Figure 5.12 Path tracking of microrobot from start point to end point using integrated system for robotic assisted PCI procedure; (a-c) selection at the first branch point. (d-f) selection at the second branch point.

VI. DICUSSIONS

Characterization of flexible microrobot based on guidewire was confirmed through several methods. These several methods are analytic solution using Euler-Bernoulli beam theory, finite element method (FEM) analysis, and experiments of actuation using magnetic field generator. Magnetic actuation of flexible microrobot composed with polydimethylsiloxane (PDMS) was able to steer at all of direction without direction axis of one's structure (Figure 5.4) and compare between results about several methods (Figure 5.5-7). The required magnetic properties for actuation in previously reported researches were magnetic field intensity of range from 30 mT to 140 mT and used relatively large-scale size of magnet. This conditions are more than twice in comparison with this research which used 15 mT magnetic field. Total tendency of comparison between magnetic field and deformation is a sine curve due to magnetic torque caused by alignment between permanent magnet and external magnetic field. Analytic solution using equation is higher than experimental results because of shorten length with relative to thickness and property of non-linear material (Equation 2-4). At the Euler Bernoulli theory, transverse stress generated at the cross section of structure was ignored in bending situation. At the fabricated microrobot, transverse stress is unable to ignore due to high slenderness ratio which is thickness to length ratio (Table 1). This transverse stress caused warping of beam structure and was less bended the beam structure. Another problem is microrobot composed with non-linear material. Polydimethylsiloxane (PDMS) material has almost 0.5 of Poisson's ratio (Table 2). Bending of flexible microrobot generate force of restoration. This force of restoration restrains to bend a tip of flexible microrobot. Analysis results with finite element method (FEM) is appropriate at the experimental results (Figure 5.5-7). Error with relative to experimental results was caused by modeling to be not consider total physical phenomenon in

actuation of flexible microrobot, truncation error due to inappropriate mesh, and non-homogeneous material.

Track-ability of flexible microrobot based on guidewire was confirmed by manipulation in blood-vessel phantom with single or multi branch (Figure 5.8-12). At the single branch blood-vessel phantom, flexible microrobot moved along the desired path under controlling magnetic field (Figure 5.8-9). Actuated head of flexible microrobot was contacted at the entrance of the desired path and moved forward to be pushing guidewire. In the phantom with high branch angle, flexible microrobot with long length and specific guidewire (GW) was successfully pass through the desired path (Figure 5.9). In the guidewire (GW) with low stiffness, pushing force was unable to delivery until beam structure which only consist of polydimethylsiloxane (PDMS) in the flexible microrobot. In the guidewire (GW) with high stiffness, tip of guidewire (GW) was moved only forward to be ignored the existence of flexible microrobot due to differentiation of stiffness between forward and backward at the connector which is brass pipe or microspring. Flexible microrobot with higher length has excellent track-ability performance in single branch model using the same guidewire (GW). Flexible microrobot based on guidewire (GW) conducted experiment in blood-vessel networks phantom (Figure 5.10). However, microrobot was designed as two degree of freedom (DOF) robot. To solve the problem which is lack of degree of freedom, microrobot based on guidewire was added the degree of freedom (DOF) using master/slave system with mechanical actuation. Flexible microrobot was controlled by two actuation using integrated system (Figure 5.11). This robot was demonstrated for a robotic assisted percutaneous coronary intervention procedure (Figure 5.12). At this demonstration, a robot reached to the desired point. Flexible microrobot was confirmed to be possible role instead of guidewire (GW). Remote controlled guidewire (GW) has advantage for surgeon and patient.

VII. CONCLUSION

7.1 Conclusion

Flexible microrobot based on guidewire (GW) for treatment of chronic total occlusion (CTO) using percutaneous coronary intervention (PCI) were designed to satisfy the condition such as magnetic actuation, flexibility, miniaturization to be more small than blood vessel, and connection with guidewire (GW). This flexible microrobot was successfully fabricated by replica molding method with polydimethylsiloxane (PDMS) mold. This flexible microrobot was steered about manipulation in all direction using external magnetic field direction with low intensity and characterized between external magnetic field and deformation using experiment, analytic solution through the equation driven by Euler-Bernoulli theory, and finite element method (FEM) analysis. This flexible microrobot based on guidewire (GW) was demonstrated in two dimensional (2D) blood vessel phantom with single or multi branch. This *in vitro* experiment of flexible microrobot was shown the actuated guidewire (GW) with higher controllability compared with conventional guidewire (GW). This research is shown the possibility of remotely controlled percutaneous coronary intervention (PCI) for intravascular treatment. A robotic-assisted percutaneous coronary intervention (PCI) procedure is able to take advantage of reduction of radiation exposure and higher success rate though convergence with robot for higher controllability of guidewire (GW).

7.2 Future work

7.2.1 Beating environment in vitro mode

Three dimensional (3D) printed blood vessel phantom for *in vitro* experiment has problems. These problems consist of space restriction for two dimensional (2D) movement, sectional phantom for targeting lesion and static fluidic flow. To applied as medical device for clinic trial or animal test should solve above mentioned limitations. Blood vessel phantom with circulating system (ELASTRAT, Switzerland) for full human body is helpful for solution (Figure 6.2). This full body phantom consist of soft material and is similar to actual blood vessel. This circulating system was fabricated as same structure compared with actual human body and has pumping function for the circulation of the fluid. Flexible microrobot based on guidewire will attempt to conduct a three dimensional (3D) *in vitro* experiment with static or dynamic flow.

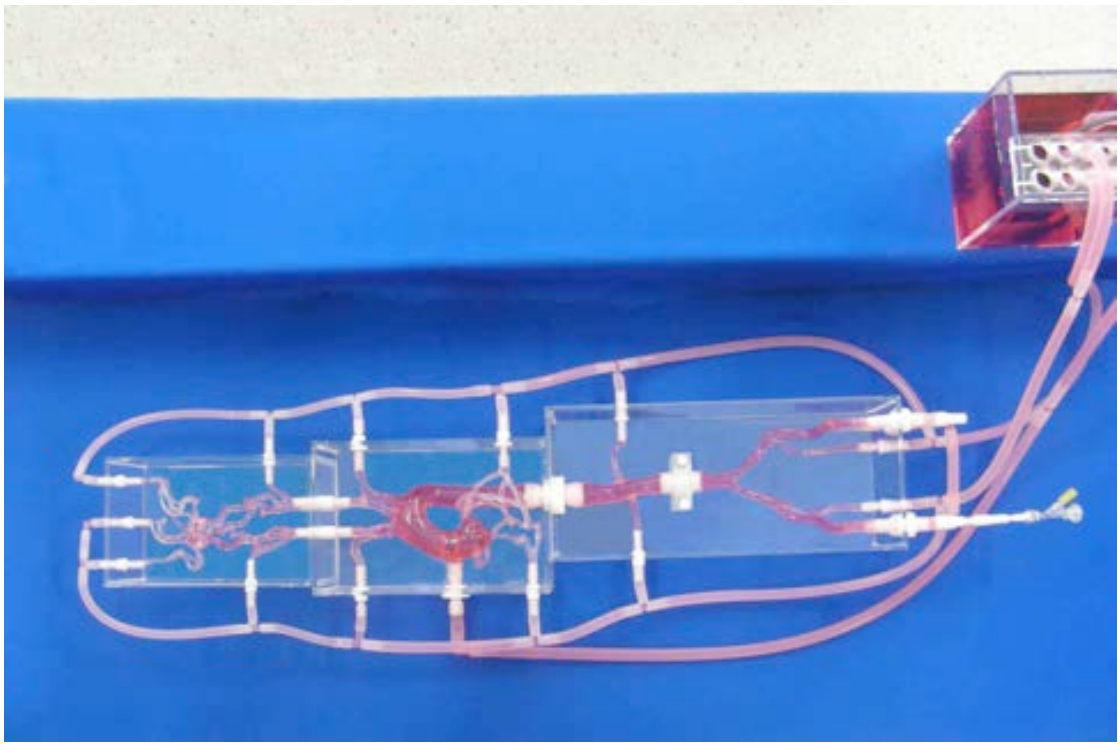

Figure 6.1 Blood vessel model of full body with beating flow

REFERENCES

[1] P. K. Whelton, L. J. Appel, R. L. Sacco, C. A. Anderson, E. M. Antman, N. Campbell, *et al.*, "Sodium, blood pressure, and cardiovascular disease further evidence supporting the american heart association sodium reduction recommendations," *Circulation*, vol. 126, pp. 2880-2889, 2012.

[2] M. J. Davies, "The pathophysiology of acute coronary syndromes," *Heart*, vol. 83, pp. 361-366, 2000.

[3] G. Touma, D. Ramsay, and J. Weaver, "Chronic Total Occlusions–Current Techniques and future directions," *IJC Heart & Vasculature*, 2015.

[4] K. Sakakura, M. Nakano, F. Otsuka, K. Yahagi, R. Kutys, E. Ladich, *et al.*, "Comparison of pathology of chronic total occlusion with and without coronary artery bypass graft," *European heart journal*, vol. 35, pp. 1683-1693, 2014.

[5] B. J. Nelson, I. K. Kaliakatsos, and J. J. Abbott, "Microrobots for minimally invasive medicine," *Annual review of biomedical engineering*, vol. 12, pp. 55-85, 2010.

[6] F. W. Mohr, M.-C. Morice, A. P. Kappetein, T. E. Feldman, E. Ståhle, A. Colombo, *et al.*, "Coronary artery bypass graft surgery versus percutaneous coronary intervention in patients with three-vessel disease and left main coronary disease: 5-year follow-up of the randomised, clinical SYNTAX trial," *The lancet*, vol. 381, pp. 629-638, 2013.

[7] Y. Fu, H. Liu, W. Huang, S. Wang, and Z. Liang, "Steerable catheters in minimally invasive vascular surgery," *The International Journal of Medical Robotics and Computer Assisted Surgery*, vol. 5, pp. 381-391, 2009.

[8] S. Suzuki, S. Furui, H. Kohtake, N. Yokoyama, K. Kozuma, and Y. Yamamoto, "Radiation exposure to patient's skin during percutaneous coronary intervention for various lesions, including chronic total occlusion," *Circulation Journal*, vol. 70, pp. 44-48, 2006.

[9] J. J. Abbott, M. C. Lagomarsino, L. Zhang, L. Dong, and B. J. Nelson, "How should microrobots swim?," *The international journal of Robotics Research*, 2009.

[10] J. Wang and W. Gao, "Nano/microscale motors: biomedical opportunities and challenges," *ACS nano*, vol. 6, pp. 5745-5751, 2012.

[11] W. Gao and J. Wang, "The environmental impact of micro/nanomachines: a review," *Acs Nano*, vol. 8, pp. 3170-3180, 2014.

[12] J.-C. Kuo, H.-W. Huang, S.-W. Tung, and Y.-J. Yang, "A hydrogel-based intravascular microgripper manipulated using magnetic fields," *Sensors and Actuators A: Physical*, vol. 211, pp. 121-130, 2014.

[13] M. Castillo-Melendez, T. Yawno, G. Jenkin, and S. L. Miller, "Stem cell therapy to protect and repair the developing brain: a review of mechanisms of action of cord blood and amnion epithelial derived cells," *Frontiers in neuroscience*, vol. 7, p. 194, 2013.

[14] M. F. Pittenger, A. M. Mackay, S. C. Beck, R. K. Jaiswal, R. Douglas, J. D. Mosca, *et al.*, "Multilineage potential of adult human mesenchymal stem cells," *science*, vol. 284, pp. 143-147, 1999.

[15] S. Kim, F. Qiu, S. Kim, A. Ghanbari, C. Moon, L. Zhang, *et al.*, "Fabrication and Characterization of Magnetic Microrobots for Three-Dimensional Cell Culture and Targeted Transportation," *Advanced Materials*, vol. 25, pp. 5863-5868, 2013.

[16] K. E. Peyer, S. Tottori, F. Qiu, L. Zhang, and B. J. Nelson, "Magnetic helical micromachines," *Chemistry–A European Journal*, vol. 19, pp. 28-38, 2013.

[17] K. E. Peyer, L. Zhang, and B. J. Nelson, "Bio-inspired magnetic swimming microrobots for biomedical applications," *Nanoscale*, vol. 5, pp. 1259-1272, 2013.

[18] S. Tottori, L. Zhang, F. Qiu, K. K. Krawczyk, A. Franco-Obregón, and B. J. Nelson, "Magnetic helical micromachines: fabrication, controlled swimming, and cargo transport," *Advanced materials*, vol. 24, pp. 811-816, 2012.

[19] S. Jeong, H. Choi, K. Cha, J. Li, J.-o. Park, and S. Park, "Enhanced locomotive and drilling microrobot using precessional and gradient magnetic field," *Sensors and Actuators A: Physical*, vol. 171, pp. 429-435, 2011.

[20] K. Khanafer, A. Duprey, M. Schlicht, and R. Berguer, "Effects of strain rate, mixing ratio, and stress–strain definition on the mechanical behavior of the polydimethylsiloxane (PDMS) material as related to its biological applications," *Biomedical microdevices*, vol. 11, pp. 503-508, 2009.

[21] F. Schneider, T. Fellner, J. Wilde, and U. Wallrabe, "Mechanical properties of silicones for MEMS," *Journal of Micromechanics and Microengineering*, vol. 18, p. 065008, 2008.

[22] I. Johnston, D. McCluskey, C. Tan, and M. Tracey, "Mechanical characterization of bulk Sylgard 184 for microfluidics and microengineering," *Journal of Micromechanics and Microengineering*, vol. 24, p. 035017, 2014.

[23] M.-Y. Cheng, C.-M. Tsao, Y.-Z. Lai, and Y.-J. Yang, "The development of a highly twistable tactile sensing array with stretchable helical electrodes," *Sensors and Actuators A: Physical*, vol. 166, pp. 226-233, 2011.

[24] X.-Y. Wang, Y. Pei, M. Xie, Z.-H. Jin, Y.-S. Xiao, Y. Wang, *et al.*, "An artificial blood vessel implanted three-dimensional microsystem for modeling transvascular migration of tumor cells," *Lab on a Chip*, vol. 15, pp. 1178-1187, 2015.

[25] Y. Guo, L. Li, F. Li, H. Zhou, and Y. Song, "Inkjet print microchannels based on a liquid template," *Lab on a Chip*, vol. 15, pp. 1759-1764, 2015.

[26] Y. Yamanishi, S. Sakuma, and F. Arai, "On-chip cell manipulation by magnetically modified soft microactuators," in *Robotics and Automation, 2008. ICRA 2008. IEEE International Conference on*, 2008, pp. 899-904.

[27] M. Riahi and E. Alizadeh, "Fabrication of a 3D active mixer based on deformable Fe-doped PDMS cones with magnetic actuation," *Journal of Micromechanics and Microengineering*, vol. 22, p. 115001, 2012.

[28] F. Khademolhosseini and M. Chiao, "Fabrication and patterning of magnetic polymer micropillar structures using a dry-nanoparticle embedding technique," *Journal of Microelectromechanical Systems*, vol. 22, pp. 131-139, 2013.

[29] L. Sun and Y. Zheng, "Bio-inspired artificial cilia with magnetic dynamic properties," *Frontiers of Materials Science*, vol. 9, pp. 178-184, 2015.

[30] B. Evans, A. Shields, R. L. Carroll, S. Washburn, M. Falvo, and R. Superfine, "Magnetically actuated nanorod arrays as biomimetic cilia," *Nano letters*, vol. 7, pp. 1428-1434, 2007.

[31] J. H. Kim, S. M. Kang, B. J. Lee, H. Ko, W.-G. Bae, K. Y. Suh, *et al.*, "Remote Manipulation of Droplets on a Flexible Magnetically Responsive Film," *Scientific reports*, vol. 5, 2015.

[32] E. Sollier, C. Murray, P. Maoddi, and D. Di Carlo, "Rapid prototyping polymers for microfluidic devices and high pressure injections," *Lab on a Chip*, vol. 11, pp. 3752-3765, 2011.

[33] H. N. Chan, Y. Chen, Y. Shu, Y. Chen, Q. Tian, and H. Wu, "Direct, one-step molding of 3D-printed structures for convenient fabrication of truly 3D PDMS microfluidic chips," *Microfluidics and Nanofluidics*, vol. 19, pp. 9-18, 2015.

[34] W. Zhang, Y. S. Zhang, S. M. Bakht, J. Aleman, S. R. Shin, K. Yue, *et al.*, "Elastomeric free-form blood vessels for interconnecting organs on chip systems," *Lab on a Chip*, vol. 16, pp. 1579-1586, 2016.

[35] N. J. Sniadecki, A. Anguelouch, M. T. Yang, C. M. Lamb, Z. Liu, S. B. Kirschner, *et al.*, "Magnetic microposts as an approach to apply forces to living cells," *Proceedings of the National Academy of Sciences*, vol. 104, pp. 14553-14558, 2007.

[36] N. Higuita Castro and D. J. Hansford, "Mechanical characterization of cells and tissues at the micro scale," *Revista Ingeniería Biomédica*, vol. 2, pp. 56-64, 2008.

[37] H. Rafii-Tari, C. J. Payne, and G.-Z. Yang, "Current and emerging robot-assisted endovascular catheterization technologies: a review," *Annals of biomedical engineering*, vol. 42, pp. 697-715, 2014.

[38] Y. Ganji, F. Janabi-Sharifi, and A. N. Cheema, "Robot-assisted catheter manipulation for intracardiac navigation," *International journal of computer assisted radiology and surgery*, vol. 4, pp. 307-315, 2009.

[39] C. Sarkissian, E. Korman, K. Hendlin, and M. Monga, "Systematic evaluation of hybrid guidewires: shaft stiffness, lubricity, and tip configuration," *Urology*, vol. 79, pp. 513-517, 2012.

[40] G. Chatzipirpiridis, P. Erne, O. Ergeneman, S. Pané, and B. Nelson, "A magnetic force sensor on a catheter tip for minimally invasive surgery," in *2015 37th Annual International Conference of the IEEE Engineering in Medicine and Biology Society (EMBC)*, 2015, pp. 7970-7973.

[41] T. Krings, J. Finney, P. Niggemann, P. Reinacher, N. Lück, A. Drexler, *et al.*, "Magnetic versus manual guidewire manipulation in neuroradiology: in vitro results," *Neuroradiology*, vol. 48, pp. 394-401, 2006.

[42] A. J. Petruska, F. Ruetz, A. Hong, L. Regli, O. Sýrýcý, A. Zemmar, *et al.*, "Magnetic needle guidance for neurosurgery: Initial design and proof of concept," in *Robotics and Automation (ICRA), 2016 IEEE International Conference on*, 2016, pp. 4392-4397.

[43] L. Muller, M. Saeed, M. W. Wilson, and S. W. Hetts, "Remote control catheter navigation: options for guidance under MRI," *Journal of Cardiovascular Magnetic Resonance*, vol. 14, p. 1, 2012.

[44] V. Lalande, F. P. Gosselin, M. Vonthron, B. Conan, C. Tremblay, G. Beaudoin, *et al.*, "In vivo demonstration of magnetic guidewire steerability in a MRI system with additional gradient coils," *Medical physics*, vol. 42, pp. 969-976, 2015.

[45] F. Settecase, M. S. Sussman, M. W. Wilson, S. Hetts, R. L. Arenson, V. Malba, *et al.*, "Magnetically-assisted remote control (MARC) steering of endovascular catheters for interventional MRI: a model for deflection and design implications," *Medical physics*, vol. 34, pp. 3135-3142, 2007.

[46] C. Liu, *Foundations of MEMS*, 2nd ed. Upper Saddle River, N.J.: Prentice Hall, 2012.

[47] M. N. Faddis, W. Blume, J. Finney, A. Hall, J. Rauch, J. Sell, *et al.*, "Novel, magnetically guided catheter for endocardial mapping and radiofrequency catheter ablation," *Circulation*, vol. 106, pp. 2980-2985, 2002.

[48] P. Kanagaratnam, M. Koa-Wing, D. T. Wallace, A. S. Goldenberg, N. S. Peters, and D. W. Davies, "Experience of robotic catheter ablation in humans using a novel remotely steerable catheter sheath," *Journal of Interventional Cardiac Electrophysiology,* vol. 21, pp. 19-26, 2008.

[49] E. S. Gang, B. L. Nguyen, Y. Shachar, L. Farkas, L. Farkas, B. Marx, *et al.*, "Dynamically shaped magnetic fields initial animal validation of a new remote electrophysiology catheter guidance and control system," *Circulation: Arrhythmia and Electrophysiology,* vol. 4, pp. 770-777, 2011.

[50] B. E. Kratochvil, M. P. Kummer, S. Erni, R. Borer, D. R. Frutiger, S. Schürle, *et al.*, "MiniMag: a hemispherical electromagnetic system for 5-DOF wireless micromanipulation," in *Experimental Robotics*, 2014, pp. 317-329.

[51] M. P. Kummer, J. J. Abbott, B. E. Kratochvil, R. Borer, A. Sengul, and B. J. Nelson, "OctoMag: An electromagnetic system for 5-DOF wireless micromanipulation," *IEEE Transactions on Robotics,* vol. 26, pp. 1006-1017, 2010.

[52] A. J. Petruska and J. J. Abbott, "Omnimagnet: An omnidirectional electromagnet for controlled dipole-field generation," *IEEE Transactions on Magnetics,* vol. 50, pp. 1-10, 2014.

[53] J. C. Simpson, J. E. Lane, C. D. Immer, and R. C. Youngquist, "Simple analytic expressions for the magnetic field of a circular current loop," 2001.

[54] A. W. Mahoney and J. J. Abbott, "Control of untethered magnetically actuated tools with localization uncertainty using a rotating permanent magnet," in *2012 4th IEEE RAS & EMBS International Conference on Biomedical Robotics and Biomechatronics (BioRob)*, 2012, pp. 1632-1637.

[55] V. N. Le, N. H. Nguyen, K. Alameh, R. Weerasooriya, and P. Pratten, "Accurate modeling and positioning of a magnetically controlled catheter tip," *Medical physics,* vol. 43, pp. 650-663, 2016.

[56] M. S. Patterson, M. T. Dirksen, A. J. IJsselmuiden, G. Amoroso, T. Slagboom, G.-J. Laarman, *et al.*, "Primary percutaneous coronary intervention by magnetic navigation compared with conventional wire technique," *European heart journal,* p. ehp587, 2010.

[57] D. J. Griffiths, *Introduction to electrodynamics*, Fourth edition. ed. Boston: Pearson, 2013.

[58] J. M. Gere and B. J. Goodno, *Mechanics of materials*, 7th ed. Toronto, ON ; Clifton Park, NY: Cengage Learning, 2009.

[59] M. Schiemann, R. Killmann, M. Kleen, N. Abolmaali, J. Finney, and T. J. Vogl, "Vascular Guide Wire Navigation with a Magnetic Guidance System: Experimental Results in a Phantom 1," *Radiology,* vol. 232, pp. 475-481, 2004.

[60] T. L. Floyd and D. M. Buchla, *Electronics fundamentals : circuits, devices, and applications*, 8th ed. Upper Saddle River, N.J.: Prentice Hall, 2010.

[61] T. L. Floyd, *Electronics fundamentals : circuits, devices, and applications,* 7th ed. Upper Saddle River, NJ: Pearson/Prentice Hall, 2007.

[62] K. Ogata, *Modern control engineering*, 5th ed. Boston: Prentice-Hall, 2010.

[63] C. Moraes, J. M. Labuz, Y. Shao, J. Fu, and S. Takayama, "Supersoft lithography: candy-based fabrication of soft silicone microstructures," *Lab on a Chip,* vol. 15, pp. 3760-3765, 2015.

[64] G. M. Whitesides, E. Ostuni, S. Takayama, X. Jiang, and D. E. Ingber, "Soft lithography in biology and biochemistry," *Annual review of biomedical engineering,* vol. 3, pp. 335-373, 2001.

[65] J. R. Anderson, D. T. Chiu, H. Wu, O. Schueller, and G. M. Whitesides, "Fabrication of microfluidic systems in poly (dimethylsiloxane)," *Electrophoresis,* vol. 21, pp. 27-40, 2000.

[66] J. C. McDonald and G. M. Whitesides, "Poly (dimethylsiloxane) as a material for fabricating microfluidic devices," *Accounts of chemical research,* vol. 35, pp. 491-499, 2002.

[67] F. Stöhr, J. Michael-Lindhard, H. Simons, H. F. Poulsen, J. Hübner, O. Hansen, *et al.*, "Three-dimensional nanometrology of microstructures by replica molding and large-range atomic force microscopy," *Microelectronic Engineering,* vol. 141, pp. 6-11, 2015.

[68] B. Da Silva, M. Zhang, G. Schelcher, L. Winter, C. Guyon, P. Tabeling, *et al.*, "Study of the Stability and Hydrophilicity of Plasma-Modified Microfluidic Materials," *Plasma Processes and Polymers,* 2016.

[69] M. Zhang, J. Wu, L. Wang, K. Xiao, and W. Wen, "A simple method for fabricating multi-layer PDMS structures for 3D microfluidic chips," *Lab on a Chip,* vol. 10, pp. 1199-1203, 2010.

[70] H.-J. Cha, H.-S. Yoon, K. Jung, B.-J. Yi, S. Lee, and J. Won, "A robotic system for percutaneous coronary intervention equipped with a steerable catheter and force feedback function," in *Intelligent Robots and Systems (IROS), 2016 IEEE/RSJ International Conference on*, 2016, pp. 1151-1156.

요 약 문

혈관 질환 치료를 위한 가이드와이어(Guidewire)기반의 의료용 마이크로로봇 제작 및 성능평가

본 연구에서는 혈관 질환을 치료하기 위해서 자기(Magnetic) 구동 가능한 가이드와이어(Guidewire) 끝단에 부착된 마이크로로봇(Microrobot)을 제작되었다. 가이드와이어, 스탠트(Stent)와 카테터(Catheter)는 동맥경화증이나 만성완전폐색병변(Chronic total occlusion, CTO)를 치료하는데 중요한 역할을 하는 의료용 도구이다. 이 중에서 가이드와이어(Guidewire)는 시술자가 손으로 돌리거나 당기거나 밀어내어 가이드와이어(Guidewire)의 끝단을 조작하여 원하는 병변의 위치까지 이동을 한다. 이러한 방식은 시술자의 숙련도나 혈관의 복잡성에 따라 긴 수술시간을 요구하며, 이로 인한 의사와 환자들에게 방사선 노출량이 증가하는 문제를 안고 있다. 이러한 원격 제어(Remote control)를 위한 카테터(Catheter)나 가이드와이어(Guidewire)는 많은 연구가 진행되었으며, 자기장을 이용한 제어는 대표적인 방식 중 하나이다. 가이드와이어의 크기로 인해 내부 자성체의 크기에 제약이 존재하며, 인체를 대상으로 하는 자기장 정밀 제어기는 전력 문제로 인해 성능의 제약을 받는다. 따라서 유연한 재질을 사용하여 낮은 자기 토크(Magnetic torque)로도 구동 되도록 설계하였다. 마이크로로봇은 제어를 위한 힘을 생성하는 자성체, 유연한 재질의 빔(Beam), 그리고 가이드와이어 끝단과의 부착을 위한 연결부(Connector)로 이루어져 있는 원기둥(Cylinder) 구조이다. 자성체는 네오디움 자석(NdFeB, N52)를 사용하였으며, 유연한 재질은 Polydimethylsiloxane (PDMS)를 이용하였으며, 연결부는 원통 구조의 황동파이프 혹은 마이크로스프링(Microspring)를 이용하였다. 이 마이크로로봇은 replica molding method 를 이용하여 성공적으로 제작되었다. 와이어 방전가공(EDM)으로 제작된 금속 몰드(Mold)를 가지고 replica molding method 를 이용하여 PDMS 몰드로 제작하였다. 만들어진 PDMS 몰드에 다른 PDMS 가 붙지않도록 표면처리를 수행하였다. PDMS 몰드 베이스(Base)에 일정한 간격을 갖는 황동파이프를 놓고, 두 파이프 사이에 영구자석을 넣는다. 이후 PDMS 몰드 커버(Cover)를 덮고, 큰 영구자석을 안에 들어가있는 자성체를 한쪽으로

이동하도록 몰드에 부착한다. 체결된 PDMS 몰드를 베이스와 경화제가 중량비 10:1 과 소량의 methylene blue 용액이 섞인 색이 띄는 PDMS 혼합액이 담긴 용기에 담아서 1 시간동안 진공챔버에 넣는다. 이후에 오븐에서 80℃에서 2 시간동안 큐어링(Curing)을 하여 경화시킨다. 몰드로부터 릴리스(Release)된 유연한 마이크로로봇은 연결부가 가이드와이어 끝단에 삽입되고 에폭시(Epoxy)로 고정시킨다. 제작된 마이크로로봇은 반구 형태에 배열된 8 개의 전자석 코일 시스템을 활용하여 자기장으로 조향 및 3D 프린팅(Printing) 혈관 모델(Model)에서의 트래킹(Tracking) 기능을 평가하였다. 제작된 마이크로로봇은 자기장을 이용해서 최대 80 도가량 모든 방향으로 꺾이는 것을 확인하고, 최대 60 도의 분지관 각도를 갖는 단일 분지관 모델에서 트래킹을 확인하였다. 이 마이크로로봇을 분석하기 위해서 오일러-베르누이 빔이론에서 도출된 비선형 방정식과 유한요소법(FEM)을 활용한 다중물리 모델을 MATLAB 과 COMSOL Multiphysics 와 같은 상용 소프트웨어(Software)를 이용하여 진행하였다. 실험, 비선형 방정식의 해, 유한요소법의 결과를 이용하여 자기장 세기와 방향에 따른 마이크로로봇의 변형각도의 관계를 그래프로 표현하였다. 가이드와이어 기반의 마이크로로봇을 다수의 분지관을 갖는 3D 프린팅된 혈관망 모델에서 자기장을 이용해 끝단을 제어하는 데모(Demo)를 보여주었다. 본 연구를 위해 제작된 가이드와이어 기반의 유연한 마이크로로봇은 가이드와이어의 역할을 수행하여 원격으로 제어하였다. 따라서 본 마이크로로봇은 혈관 치료를 위한 로봇 보조 관상동맥 중재술(Robotic assisted percutaneous coronary intervention (PCI))의 가능성을 갖고 있다.

핵심어: Flexible microrobot, Replica molding method, Magnetic actuation, Finite element method (FEM), Intravascular treatment.

APPENDIX

A.1 Stainless steel mold for replica molding method using wire electric discharge machining

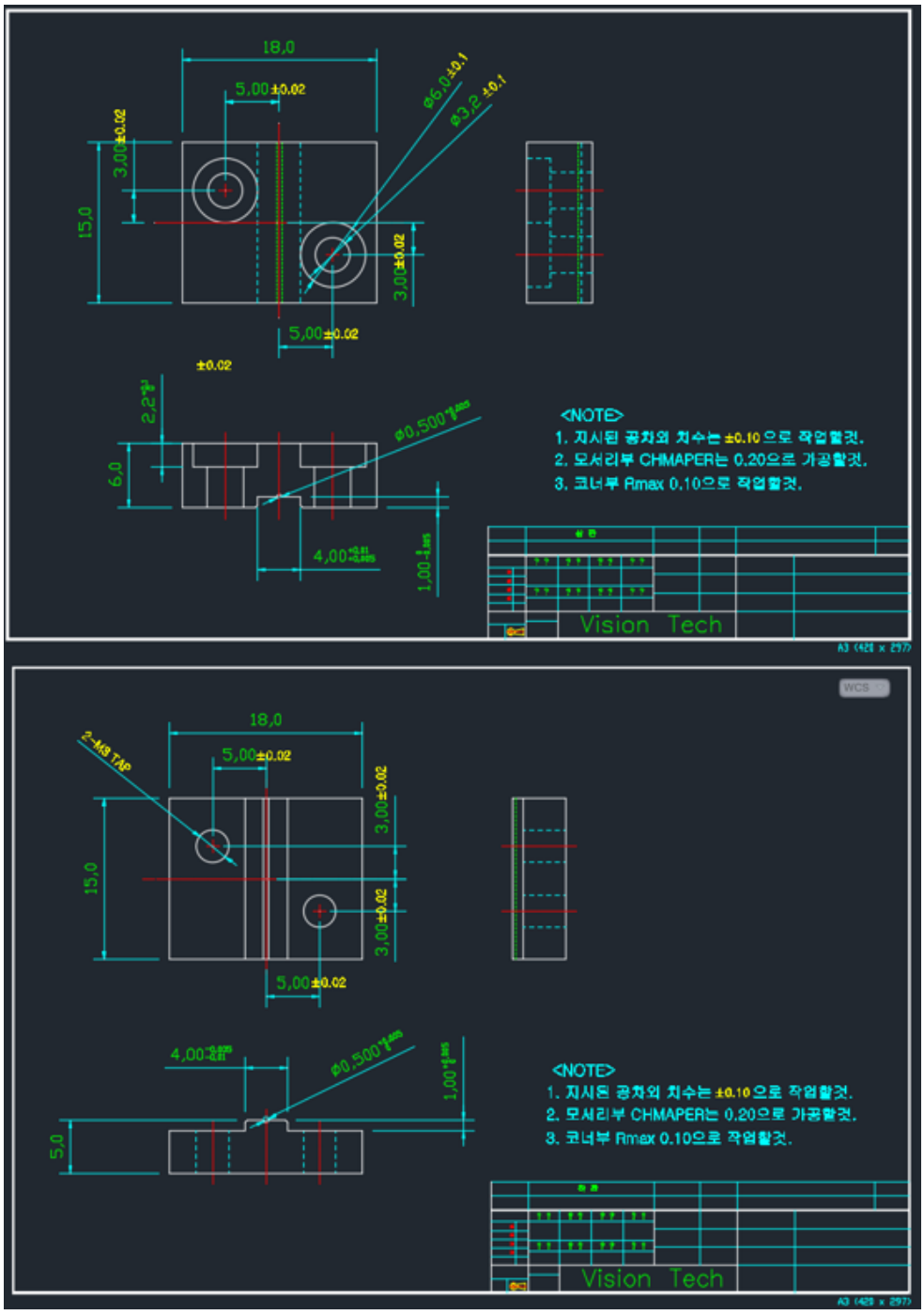

Figure A.1 Design of stainless steel mold for replica molding method

A.2 MATLAB code for analytic solution

```
%% parameter for simulation
% Geomery and property of Permanent magnet and PDMS
M=1.43e6;                % Magnetization of NdFeB magnet[A/m]
D=400e-6;                % Diameter of NdFeB magnet [m]
L=800e-6;                % Length of NdFeB magnet [m]
m_single=M*pi/4*D^2*L;   % Magnetic moment of NdFeB magnet [A*m^2]
E=750e3;                % Young's modulus of PDMS material [Pa(N/m2)]
Di=500e-6;               % Diameter of cylinderical PDMS beam [m]
Li=3000e-6;              % Length of cylinderical PDMS beam [m]
Iz=pi/64*Di^4;           % 2nd moment of inertia of Cylinderical PDMS beam [m^4]
% variables of simulation
B=[5e-3, 10e-3, 15e-3]; % Strength of magnetic field [T]
Gamma=0:1:180;          % direction of magnetic field [Deg]

%% Calculation - Fixed point iteration method
Ni=length(Gamma);
Nj=length(B);
Theta=zeros(Ni,Nj);
for i=1:Ni;
    for j=1:3;
        gamma=Gamma(i)*pi/180;
        syms th
        assume(th >= 0)
        [th]=solve(th==m_single*B(j)*Li/(E*Iz)*sin(gamma-th),th);
        Theta(i,j)=double(th)*180/pi;
    end
end
data=[Gamma',Theta];
xlswrite('data.xls',data);

%% ploting
plot(Gamma,Theta)
xlabel('Magnetic field direction [Deg]')
ylabel('Defored angle [Deg]')
```

Figure A.2 MATLAB code for analytic solution

A.3 Manual Procedure for COMSOL setting

A.3.1 Modeling Setting

(a) Go to the **Model Wizard** window.

(b) Click the **2D** button and **Next**.

(c) In the Add **physics** tree, select three items.

- AC/FC > Magnetic Fields, No Currents (mfnc)

- Structural Mechanics > Solid Mechanics (solid)

- Mathematics > Deformed Geometry > Moving Mesh (ale)

(d) Click the **Next**.

(e) In the **Studies** tree, select **Preset Studies > Time Dependent**.

(f) Click **Done**.

A.3.2 Set-up Global Parameter

(a) In the **Model Builder** window, right-click **Global Definitions** and Choose **Parameters**.

(b) Go to the **Settings** window for Parameters.

(c) Locate the **Parameters** section. In the **Parameters** table, enter the following settings:

Table 5. Parameters of Global Definitions for COMSOL setting

NAME	EXPRESSION	DESCRIPTION
L_PDMS	3[mm]	PDMS beam length
D_PDMS	0.5[mm]	PDMS beam diameter
L_mag	0.8[mm]	Magnet length
D_mag	0.4[mm]	Magnet diameter

L_work	30[mm]	Working area for uniform magnetic field
B_mag	15[mT]	Magnetic field strength
B_dir	T[1/s]*1[deg]	Time dominant direction of magnetic field
L_tot	L_PDMS+L_mag+5[um]	Total length of microrobot
Gap	1[mm]	Boundary gap for formation of far field

A.3.3 Geometry 1

(a) In the **Model Builder** window, right-click **Model 1>Geometry 1** and choose **Square**

Table 6. Geometry of five square; Side section and Position section

NAME	Side length	x	y
Square 1 (*sq1*)	L_work-Gap	0	0
Square 2 (*sq2*)	Gap	L_work/2	L_work/2
Square 3 (*sq3*)	Gap	-L_work/2	L_work/2
Square 4 (*sq4*)	Gap	-L_work/2	-L_work/2
Square 5 (*sq5*)	Gap	L_work/2	-L_work/2

(b) In the **Model Builder** window, right-click **Model 1>Geometry 1** and choose **Rectangle**

Table 7. Geometry of six rectangles; Size and Shape section and Position section

NAME	Width	Height	x	y
Rectangle 1 (*r1*)	L_tot	D_PDMS	-L_tot/2	-D_PDMS/2
Rectangle 2 (*r2*)	L_mag	D_mag	-L_tot/2+L_PDMS	-D_mag/2
Rectangle 3 (*r3*)	L_work-gap	gap	0	L_work/2
Rectangle 4 (*r4*)	L_work-gap	gap	0	-L_work/2
Rectangle 5 (*r5*)	L_work-gap	gap	L_work/2	0
Rectangle 6 (*r6*)	L_work-gap	gap	-L_work/2	0

(c) In the **Model Builder** window, right-click **Form Union** and choose **Build Selected**.

A.3.4 Definitions

(a) In the **Model Builder** window, right-click **Model 1>Definitions** and choose **Infinite Element Domain**.

(b) Select Domain 1, 2, 3, 4, 6, 9, 10, 11.

A.3.5 Materials

1. Air

(a) In the **Model Builder** window, right-click **Model 1>Materials** and choose **Add Material**.

(b) Select **Built-In>Air**.

(b) Select Domain 1, 2, 3, 4, 5, 6, 9, 10, 11.

(c) Go to the **Settings** window for Air.

(d) Locate the **Material Contents** section. In the **Relative permeability** edit filed, type 1.

2. PDMS - Polydimethylsiloxane

(a) Choose **Add Material**.

(b) Select **MEMS>Polymers>PDMS - Polydimethylsiloxane**.

(c) Select Domain 7 only.

(d) Go to the **Settings** window for PDMS - Polydimethylsiloxane.

(e) Locate the **Material Contents** section. In the **Density** edit filed, type 970.

(f) In the **Relative permeability** edit filed, type 1.

3. NdFeB – Neodymium Magnet

(a) In the **Model Builder** window, right-click **Model 1>Materials** and choose **Blank Material**.

(b) In the **Label** edit field, type NdFeB.

(c) Select Domain 8 only.

(d) Go to the **Settings** window for NdFeB.

(e) Locate the **Material Contents** section. In the **Young's modulus** edit filed, type 160[GPa].

(f) In the **Poisson's ratio** edit filed, type 0.24.

(g) In the **Density** edit filed, type 7500.

A.3.6 Magnetic Fields, No Currents

1. Magnetic Fields, No Currents (*mfnc*)

(a) In the **Model Builder** window, click **Model 1>Magnetic Fields, No Currents**

(b) Go to the **Settings** Window for Magnetic Fields, No Currents.

(c) Select Domain 1~11.

(d) Locate the **Background Magnetic Field** section. In the **Background magnetic field** edit field, specify the $\boldsymbol{H_b}$ vector as

Table 8. Background magnetic field

B_mag/mu0_const*cos(B_dir)	x
B_mag/mu0_const*sin(B_dir)	y
0	z

2. External Magnetic Flux Density 1

(a) Right-click **Magnetic Fields, No Currents** and choose **External Magnetic Flux Density**.

(b) Select Boundary 10, 11, 13, 25.

3. Zero Magnetic Scalar Potential 1

(a) Right-click **Magnetic Fields, No Currents** and choose **Zero Magnetic Scalar Potential**.

(b) Select Point 1, 4, 21, 24.

4. Magnetic Flux Conservation 2

(a) Right-click **Magnetic Fields, No Currents** and choose **Magnetic Flux Conservation**.

(b) Select Domain 8 only.

(c) Locate the **Material type** section. From the **Material type** list, select **Solid**.

(d) Locate the **Magnetic Field** section. From the **Constitutive relation** list, select **Remanent flux density**.

(e) Locate the **Relative permeability** section**.** In the $\boldsymbol{\mu_r}$ edit field, type User defined, 2, Isotropic.

(f) In the **Remanent flux density** edit field**,** specify the $\boldsymbol{B_r}$ vector as, type 1.43, 0, 0.

Table 9. Renemanent flux density

1.43	x
0	y
0	z

5. Force Calculation 1

(a) Right-click **Magnetic Fields, No Currents** and choose **Force Calculation**.

(b) Select Domain 8 only.

A.3.7 Solid Mechanics

1. Solid Mechanics (*solid*)

(a) In the **Model Builder** window, click **Model 1>Solid Mechanics**

(b) Go to the **Settings** Window for Solid Mechanics.

(c) Locate the **Thickness** section. In the *d* edit field, type D_mag.

(d) Locate the **Structural Transient Behavior** section. From the list, select **Quasi-static**.

2. Fixed Constraint 1

(a) Right-click **Solid Mechanics** and choose **Fixed Constraint**.

(b) Select Boundary 15 only.

3. Boundary Load 1

(a) Right-click **Solid Mechanics** and choose **Boundary load**.

(b) Select Boundary 18, 19, 20, 21.

(c) Locate **Force** section. From the **Load type** list, select **Load defined as force per unit area**.

(d) And from the **Fa** list, select **Maxwell surface stress tensor**.

A.3.8 Moving Mesh

1. Moving Mesh (*ale*)

(a) In the **Model Builder** window, click **Model 1>Moving Mesh**

(b) Go to the **Settings** Window for Moving Mesh.

(c) Select Domain 5, 7, 8.

(d) Locate **Free Deformation Settings** section. From **Mesh smoothing type** list, select Yeoh

(e) In the **Stiffening factor** edit field. type 100.

2. Free Deformation 1

(a) Right-click **Moving Mesh** and choose **Free Deformation**.

(b) Select Domain 5, 7, 8.

3. Prescribed Mesh Displacement 2

(a) Right-click **Moving Mesh** and choose **Prescribed Mesh Displacement**

(b) Select Boundary 16 ~ 22.

(c) Locate **Prescribed Mesh Displacement** section.

(d) Check **Prescribed x displacement** and $\boldsymbol{d_x}$ edit field, type u.

(e) Check **Prescribed y displacement** and in the $\boldsymbol{d_y}$ edit field, type v.

4. Prescribed Mesh Displacement 3

(a) Right-click **Moving Mesh** and choose **Prescribed Mesh Displacement**

(b) Select Boundary 15 only.

(c) Locate **Prescribed Mesh Displacement** section.

(d) Check **Prescribed x displacement** and $\boldsymbol{d_x}$ edit field, type 0.

(e) Check **Prescribed y displacement** and in the $\boldsymbol{d_y}$ edit field, type 0.

A.3.9 Meshes

1. Free Triangular 1

(a) Right-click **Mesh** and choose **Free Triangular**.

(b) Locate **Domain Selection** section. From **Geometric entity level** list, select Domain.

(c) Select Domain 8 only.

(d) Right-click **Free Triangular** and choose **Size**.

(e) Locate **Element Size** section. In the **Calibrate for** edit field, check Custom.

(f) Locate **Element Size Parameters** section. Check **Maximum element size** and type 60 [um].

2. Free Triangular 2

(a) Right-click **Mesh** and choose **Free Triangular**.

(b) Locate **Domain Selection** section. From **Geometric entity level** list, select Domain.

(c) Select Domain 7 only.

(d) Right-click **Free Triangular** and choose **Size**.

(e) Locate **Element Size** section. In the **Calibrate for** edit field, check Custom.

(f) Locate **Element Size Parameters** section. Check **Maximum element size** and type 60 [um].

(g) Locate **Element Size Parameters** section. Check **Resolution of narrow regions** and type 2.

3. Free Triangular 3

(a) Right-click **Mesh** and choose **Free Triangular**.

(b) Locate **Domain Selection** section. From **Geometric entity level** list, select Domain.

(c) Select Domain 5 only.

(d) Right-click **Free Triangular** and choose **Size**.

(e) Locate **Element Size** section. In the **Calibrate for** edit field, check Custom.

(f) Locate **Element Size Parameters** section. Check **Maximum element size** and type 1500 [um].

4. Mapped 1

(a) Right-click **Mesh** and choose **Mapped**.

(b) Locate **Domain Selection** section. From **Geometric entity level** list, select Remaining.

(c) Right-click **Mapped** and choose **Distribution**.

(d) Select Boundary 1, 2, 5, 7, 24, 29, 30, 32.

(e) Locate **Distribution** section. In the **Number of elements** edit field, type 5.

A.3.10 Study

1. Step1: Time Dependent

(a) In the **Model Builder** window, expand the **Study 1** node, then click **Step 1: Time Dependent**.

(b) Go to the **Settings** window for Time Dependent, locate the **Study Settings** section.

(c) In the Times text field, type range(0,10,170).

(d) Select the **Relative tolerance** check box and in the associated text field, type 0.01.

(e) Select the **Include geometric nonlinearity** check box.

(f) Locate the **Study Extensions** section, select the **Automatic remeshing** check box.

2. Solver Configurations

(a) In the **Model Builder** window, expand the **Study 1 > Solver Configurations > Solution 1 > Time-Dependent Solver 1** node. Click **Fully Coupled**.

(b) Locate **Method and Termination** section. From **Jacobian update** list, select On every interation.

(c) In the **Maximum number of interations** text field, type 25.

(d) In the **Time Dependent Solver**, Click **Automatic Remeshing**.

(e) Locate **Condition for Remeshing** section. From **Condition type** list, select **Mesh quality**.

(f) In the **Stop when mesh quality is below** text field, type 0.15.

A.3.11 Results

1. Image of Distribute Magnetic field

(a) In the **Model Builder** window, right-click **Results** and choose **2D plot Group**.

(b) In the **2D plot Group** window, right-click **surface**.

(c) In the **Settings** window for surface, Click **Replace Expression**.

(d) From the menu, choose **Component 1 > Magnetic Fields, No Current > Magnetic > Reduced Magnetic field (Spatial) > mfnc.normB – Magnetic flux density norm**.

(e) On the **2D plot Group** window, click **Plot**.

2. Data of deformed angle according to magnetic field

(a) In the **Model Builder** window, right-click **Results > Derived Values** and choose **Point Evaluation**.

(b) Go to the **Settings** window for Point Evaluation, locate the **Selection** section.

(c) Select Point 12, 14.

(d) In the **Expression** section, click **Replace Expression**.

(e) From the menu, choose **Component 1 > Geometry > Coordinate (Spatial) > x-coordinate** and **y-coordinate**, relatively.

(f) Click the **Evaluate** button.